https://doi.org/10.5194/egusphere-2025-6553
Preprint. Discussion started: 8 January 2026

Insights into the low-level single-layer stratiform cloud optical depth feedback based on two decades of observations at the North Slope of Alaska

Calvin Coulbury[1], Ivy Tan[2], David Turner[3], and Chen Zhou[4]

[1]Department of Atmospheric and Oceanic Science, McGill University, Montreal, QC, Canada, H3A 0B9
[2]Department of Physics, University of Colorado Boulder, Boulder, CO, USA, 80302
[3]National Oceanic and Atmospheric Administration, Global Systems Laboratory, Boulder, CO, USA, 80305
[4]School of Atmospheric Sciences, Nanjing University, Nanjing, Jiangsu, China, 210093

Correspondence: Calvin Coulbury (calvin.coulbury@mail.mcgill.ca)

Abstract. A 21 year dataset of cloud optical depth (COD) over Utqiagvik, AK is retrieved from longwave (LW) Atmospheric Emitted Radiance Interferometer (AERI) observations. Cloud property changes with temperature, time, and other meteorological variables are investigated. We find that the COD of low-level, single-layer optically thin, stratiform, Arctic clouds at pressures greater than 680 hPa increases with warming for column averaged atmospheric temperatures between $-16°C$ and $-4°C$, while the COD decreases with warming between $-4°C$ and $0°C$, with little change below $-16°C$. This aligns with current literature. COD changes are driven by liquid water content (LWC) variations with temperature, with additional contributions from cloud physical thickness (CPT) changes and bulk cloud phase shifts. The COD of summer and winter clouds decreases with warming at all observed temperatures, while the COD of spring and autumn clouds increases with warming. We extend existing literature with a cloud controlling factor (CCF) analysis, finding that the atmospheric temperature at 850 hPa; the surface windspeed; and sea salt, sulfur dioxide and hydrophilic organic carbon concentrations are important controls on the COD. The length of the dataset allows us to perform novel trend investigation, with statistically significant positive trends found in the total (0.0824 year^{-1}) and liquid (0.0719 year^{-1}) CODs. Evidence is provided for a negative surface cloud feedback. Our results and associated dataset represent an avenue for the evaluation and improvement of model representations of Arctic cloud microphysical processes.

1 Introduction

Arctic amplification (AA) is the observed phenomenon of elevated warming at high northern latitudes as compared to the rest of the globe, most prominent in the autumn and winter (Manabe and Stouffer, 1980; Taylor et al., 2022; Rantanen et al., 2022). While the main drivers of AA are broadly understood (Pithan et al., 2014; Dai et al., 2019; Jenkins and Dai, 2021), our ability to project the magnitude of this phenomenon into the future is precluded by a poorly constrained cloud feedback (Hahn et al., 2021; Previdi et al., 2021). The different components of the cloud feedback are typically understood by decomposition into changes in cloud fraction (CF), cloud top pressure (CTP), and cloud optical depth (COD) (Zelinka et al., 2012), each of which has complex and often competing effects on the climate system (Ceppi et al., 2017). The largest source of uncertainty in model

https://doi.org/10.5194/egusphere-2025-6553
Preprint. Discussion started: 8 January 2026

projections of Arctic amplification is the cloud feedback, and within projections of the cloud feedback, the largest source of uncertainty comes from changes in COD with warming (Taylor et al., 2022). Additionally, the sign of the median SW Arctic cloud feedback changed from negative to positive between CMIP5 and CMIP6 models, driven in large part by a less negative COD feedback (Coulbury and Tan, 2024).

Projections of the COD feedback in the Arctic have a large uncertainty due to disagreements between global climate models on how to parameterize cloud processes such as INP activation, the Wegener-Bergeron Findeisen process, and other small scale cloud microphysical processes (Gettelman and Sherwood, 2016; Tan et al., 2016, 2022). This results in large biases in the COD feedback in the Arctic and elsewhere for multiple reasons. For a similar amount of water, liquid clouds tend to have a larger COD than ice clouds, therefore disagreements on the phase distribution of water in mixed-phase clouds and the occurrence of liquid and ice phase clouds individually have important impacts on the COD (Sun and Shine, 1994). These disagreements also have a large impact on the cloud phase feedback. The cloud phase feedback is the process in which climates with icier clouds will have a more negative COD feedback than climates with less icy clouds, for the same amount of warming, due to the transition from ice to liquid particles being associated with increasing COD (Tan et al., 2019). Disagreements on cloud microphysical process parameterizations result in inter-model discrepancies in the representation of cloud phase, COD, and its associated feedback processes. This in turn causes large inter-model spread in simulated AA and Equilibrium Climate Sensitivity (ECS) values (Tan et al., 2016, 2022).

The lack of agreement between models on how to parameterize cloud properties comes in part from a lack of reliable and consistent observations. There have been observational field campaigns targeting Arctic clouds, but their spatiotemporal extent is often limited. Passive satellite observations are limited by both the optical and thermal similarity of Arctic clouds to sea ice and the necessity of sunlight (Liu et al., 2009; Chan and Comiso, 2013), while active satellite observations are limited in swath, temporal coverage, and have difficulty observing low clouds in multilayered cloud scenes or due to ground clutter when using active radar (Winker et al., 2009; Blanchard et al., 2014). Surface based observations are better suited to gathering data on low-level, stratiform clouds which are relevant to the surface radiation balance in the Arctic due to their proximity to the surface and their ubiquity in the Arctic environment (Mioche et al., 2017).

One way to address model disagreements is to use surface based observations of COD to constrain model representations of the COD feedback through the property of timescale invariance. COD changes with temperature, and it does so at a rate depending largely on the temperature of the environment that the clouds exist in (Tseloudis et al., 1992; Gordon and Klein, 2014). It has been posited that this is because changes in COD are controlled in large part by thermodynamic principles, and as such COD reacts similarly to temperature changes regardless of the timescale over which these temperature changes occur. The COD is therefore considered to be timescale invariant. Using model realizations representing both a pre-industrial atmosphere and an atmosphere with elevated carbon dioxide concentration, Gordon and Klein (2014) demonstrated that COD changes in a control climate can be used to make conclusions about the long-term COD feedback in a perturbed climate.

Observational analyses have provided evidence to constrain the timescale invariant COD feedback in the Arctic (Terai et al., 2019) and elsewhere (Tseloudis et al., 1992), but only over a relatively limited observational period. Additionally, Tan et al. (2019) developed a framework to decompose changes in COD with temperature into contributions from each cloud

https://doi.org/10.5194/egusphere-2025-6553
Preprint. Discussion started: 8 January 2026

phase. Extending this existing framework, we analyze how COD over the U.S. Department of Energy's Atmospheric Radiation Measurement site on the North Slope of Alaska (NSA) in Utqiagvik, AK (Verlinde et al., 2016) changes with temperature in a 21 year dataset and investigate the long-term cloud feedback in the real-world Arctic, with the goal of improving our understanding of the COD feedback and associated cloud microphysical processes. This work represents the extension of previous literature in the domain of COD timescale invariance to climate temporal scales. We use an optimal estimation-based algorithm, the Mixed-phase Cloud Retrieval Algorithm (MIXCRA; Turner (2005)) to produce a 21-year dataset of COD, water path, and effective radius of liquid, ice, and mixed phase clouds. We limit ourselves to stratiform clouds to cater to the strengths of the MIXCRA algorithm, discussed in more detail below. The methods for both the retrieval of our dataset using MIXCRA and the subsequent analysis of the dataset are presented in Section 2, the results of this analysis are presented in Section 3, and these results are summarized, synthesized, and discussed in Section 4.

2 Methods

2.1 The Atmospheric Emitted Radiance Interferometer

The Atmospheric Emitted Radiance Interferometer (AERI) measures downwelling spectral infrared radiance between 3.3 and 25 μm with 1 cm^{-1} resolution (Knuteson et al., 2004a, b). The AERI was developed in the 1990s primarily to address the scientific goals of the Department of Energy's Atmospheric Radiation Measurement (ARM) program (Turner et al., 2016). The AERI regularly views two well-characterized blackbody targets, which are operated at different temperatures, allowing the instrument to observe downwelling radiance with a radiometric accuracy better than 1% of the ambient radiance (Knuteson et al., 2004b). An AERI has been deployed more-or-less continuously at the NSA site since its inception.

Infrared radiance is very sensitive to cloud properties (Mace et al., 1998; Deslover et al., 1999), and thus changing cloud properties during the sky viewing period would result in complicated radiance spectra that are difficult to analyze. The development of a principal-component based noise filter (Turner et al., 2006) allowed for the reduction of the sky viewing period from one 3.5 minutes every 7 minutes to one 12 second view every 230 seconds. This "rapid-sample" strategy reduces the likelihood of complicated scenes where different cloud properties are convolved into a single infrared radiance observation. All AERI data collected by ARM are processed with this noise filter.

2.2 Retrieval of Cloud Optical Depth via The MIXCRA Algorithm

We utilize the Mixed-phase Cloud Retrieval Algorithm (MIXCRA; Turner (2005)) to retrieve cloud properties from the observed AERI radiance spectra. MIXCRA takes advantage of the differences in the refractive indices of liquid water and ice in the 8 to 25 μm region to identify the cloud optical depths (COD) of the liquid and ice components of the cloud, as well as the effective radius of both phases ($r_{eff,liq}$ and $r_{eff,ice}$, respectively). From the COD and r_{eff} values, the liquid water path (LWP) and ice water path (IWP) can be estimated.

https://doi.org/10.5194/egusphere-2025-6553
Preprint. Discussion started: 8 January 2026

MIXCRA uses an optimal-estimation approach (Rodgers, 2000; Maahn et al., 2020), which allows uncertainties in the observations and the sensitivity of the forward model to be propagated to provide uncertainties in the retrieved cloud properties. Several components of this algorithm are critical for its operation. An optimal estimation framework needs a forward model, from which the atmospheric state can be used to generate a synthetic observation. In MIXCRA the atmospheric state is the cloud properties of the observed scene while the synthetic observation is a simulated AERI spectrum. We use the LBLDIS model (Turner, 2003), which uses the Line-By-Line Radiative Transfer Model (LBLRTM (Clough et al., 2005)) to compute the spectral gaseous optical depths and the Discrete Ordinates Radiative Transfer code (DISORT; Stamnes et al. (1988)) to compute the downwelling radiance. DISORT allows for both emission and scattering, and thus is a full 1-dimensional radiative transfer framework.

The refractive indices of liquid and ice must be processed to provide optical scattering and emission coefficients of cloud properties. Assuming spherical cloud particles, Mie theory has been used to compute these optical properties for a range of particle sizes for each of the AERI wavelengths. These scattering properties are then integrated over a size distribution, which is assumed to be a gamma distribution (Turner, 2005), and then stored in a single scattering property (SSP) database that is used as a lookup table by LBLDIS. Ice particles are non-spherical, and the optical properties of ice depend on their habit. The optical properties by Yang et al. (2005) were also integrated over a gamma size distribution for different effective radii, and stored into habit-dependent SSP databases. However, many of these habits have similar effective density as spheres, and thus result in similar values for ice COD as when the ice particles are assumed to be spherical. Note that smaller ice particles in both deep stratus and cirrus Arctic clouds have been observed to be spheroids (Lawson et al., 2001; Wolf et al., 2018). As ice particles grow, they can become non-spherical and often fractal in nature, resulting in a low ice density, and Grenfell and Warren (1999) demonstrated that retrievals in these types of conditions usually preserve the ratio of volume to projected area of the crystals, not the number density, and thus the retrieved size is usually much smaller than the actual size of the ice crystal. Thus, while our analysis is focused on optically thinner, low-level stratus clouds that likely encompass a range of ice habits, we assume that the ice habit is spherical.

MIXCRA can be run assuming that the AERI is observing either a dual-phase cloud, which would contain both liquid and ice, or a single phase cloud. The dual-phase model works well if the precipitable water vapor is less than 1 cm, thereby allowing the atmosphere to be semi-transparent in the far infrared wavelengths (18 to 25 μm) (Turner, 2003), and if the total COD is larger than approximately 0.3. If it is a certainty that the cloud is only a single phase, then the accuracy of the retrieved cloud properties is higher when MIXCRA is run in single-phase mode. For our analysis, MIXCRA was run by default in dual-phase mode, but if the cloud is determined to be warmer than 0 $^{\circ}C$ or colder than -40 $^{\circ}C$, then MIXCRA automatically converts to a single-phase retrieval (liquid or ice, respectively).

When the retrieval is run, it first applies a simple quality control check to the observed AERI radiance spectrum (Y) to eliminate bad observations. The radiance at 900 cm^{-1} must be above -10 $mW(m^2 srcm)^{-1}$ (which is -10 RU, henceforth). To run the retrieval, profiles of pressure, temperature, and water vapor from temporally interpolated radiosondes (launched every 6 hours) are used to compute the gaseous optical depth spectra as a function of height. A first-guess of the liquid and ice COD and r_{eff} values is made, representing our desired retrieved product, the state vector $X = [COD_{liq}, COD_{ice}, r_{eff,liq}, r_{eff,ice}]$.

https://doi.org/10.5194/egusphere-2025-6553
Preprint. Discussion started: 8 January 2026

This is combined with the cloud base height from a co-located ceilometer and the user-specified SSP databases to provide the optical properties of the cloud at the right altitude for the LBLDIS forward model. The simulated downwelling radiance, F(X), is then compared to Y. An update of the state vector (X_{n+1}) is computed using the sensitivity of the forward model Jacobian $K = \partial F/\partial X_n$ and weighted by the uncertainty of the observations, which is given by the covariance matrix S_m as in

$$X_{n+1} = X_n + \left(S_a^{-1} + K^T S_m^{-1} K\right)^{-1} \left(K^T S_m^{-1} \left(Y - F(X_n) - S_a^{-1}\left(X_n - X_a\right)\right)\right), \tag{1}$$

from Rodgers (2000), Eq. 5.8. We compute K using finite differences. The prior climatology of cloud properties is not known, and thus the uncertainty of the prior S_a is set so that the assumed prior provides no constraint when the retrieval is in dual-phase mode. S_a is assumed to be a diagonal matrix such that there is no covariance between the CODs of the two phases, or correlations between the particle sizes of either phase with each other or with COD. However, if the retrieval is in single-phase mode, then the mean prior COD for the undesired phase is set to zero, meaning X_a has the same structure as X above, and the uncertainty for that term is set to be small (roughly 1×10^{-8}).

A benefit of the optimal estimation framework is that the uncertainty of the retrieved cloud properties X is given the via the covariance matrix S_x, where

$$S_x = \left(S_a^{-1} + K^T S_m^{-1} K\right)^{-1}. \tag{2}$$

The square root of the diagonal of S_x is the 1-sigma uncertainty in the retrieved values of the liquid COD, ice COD, and liquid and ice r_{eff} respectively. The ability of MIXCRA to discriminate cloud phase and COD has been evaluated using a high-spectral resolution LIDAR (Turner and Eloranta, 2008).

Once this optimal estimation has been applied to every available AERI observation, post-processing is performed to ensure high quality retrievals. The first level of quality control performed on the data is to remove the impacts of two known instrument issues. First, there is a metal hatch on the AERI to protect the observation equipment from fouling during precipitation events. The controller of this hatch, which also records its status, malfunctioned several times over the period between July 2006 and February 2008 (Zwink and Turner, 2012). While it is not possible to determine with complete certainty for what observation periods the hatch was completely open, Zwink and Turner (2012) developed a neural network to determine with high accuracy which points should be kept and discarded over this time period. Points for which the hatch was determined to be completely open by this neural network were kept, with all other timesteps discarded. The second instrument issue occurred between May 15th and December 1st 2011. During this time an instrument swap was occurring, and a standard range AERI was used whose output is not suitable for our retrieval as the maximum wavelength observed was $19\mu m$, while dual-phase cloud retrievals greatly benefit from having observations in the $19\mu m$ to $25\mu m$ band. This period has been discarded completely.

Realistic quality control limits are applied to the data to remove unphysical values. Optimal estimation is a purely mathematical process, and solutions to the retrieval may be mathematically correct but not physically possible. Data points are included or excluded based on 5 reported values at each time-step: the summed liquid and ice COD, the LWP, the root mean

https://doi.org/10.5194/egusphere-2025-6553
Preprint. Discussion started: 8 January 2026

square error between the final simulated AERI spectra and the AERI observation, the liquid particle effective radius, and the ratio of the COD to its uncertainty. To restrict ourselves to realistic points, any time-step for which the total COD exceeds 50 or the LWP exceeds $100gm^{-2}$ is discarded. For clouds with large COD, the LW spectra becomes saturated and the COD cannot be reliably retrieved (Turner, 2007). We also discard points for which the root mean square error between the AERI observation and the forward model is greater than $2RU$. This removes points for which the simulated observation differed strongly from the observed radiance, which usually occurs when the maximum of 10 iterations of the optimal estimation process were performed. Additionally, points for which the effective radius of liquid particles in the cloud is outside of the range $3.5\mu m < r_{eff,liq} < 20\mu m$ are discarded. The low restriction is required because if the MIXCRA algorithm determines that there is a near zero LWP but a non-zero liquid COD it assumes that the liquid particles in the cloud have near zero radius. The high limit is put in place to avoid precipitating scenes. When the retrieved $r_{eff,liq}$ exceeds $20\mu m$ there is a high likelihood that drizzle would be occurring, indicating that the retrieval is unphysical because the observation hatch should be closed during precipitation events. The final restriction, that the ratio of the uncertainty in the COD to its magnitude $\left(\frac{\sigma_{liq}+\sigma_{ice}}{\tau_{liq}+\tau_{ice}}\right)$ must be less than 0.15 focuses the accuracy of our dataset on the COD. This ensures that the retrieval is reasonably certain of the values of the points we report. Once these limits have been applied we use the ice COD and effective radii, along with Eq. 8 of (Turner, 2005), from Stephens (1994), to calculate the IWP, propagating the error in each of these values to determine the uncertainty in the IWP. Characteristics of this retrieved dataset can be found in Sect. 3.1.

While the temporal resolution of the MIXCRA retrieval is nominally every 20 seconds, we report the dataset on several time resolutions and it is necessary to understand that multiple clouds may be averaged together when considering larger time-steps. For all analyses in this manuscript, unless explicitly labeled otherwise, the data are temporally averaged at a monthly level using only single-layer stratiform clouds for which the CTP is greater than 680 hPa. These limitations are applied because the MIXCRA algorithm is best suited to retrieving properties of low, optically thin, single-layer clouds. We use the cloud mask developed in Stauffer et al. (2025) to isolate these points. Focus on low, stratiform, optically thin clouds is merited given that small changes in LWP, specifically when the LWP of a cloud is small, result in relatively large changes in the radiative fluxes of the atmospheric column in which the cloud exists (Fig. A1, and Turner et al. (2007)).

2.3 Analysis of Cloud Optical Depth Dataset

2.3.1 Quantifying the Cloud Radiative Effect and Cloud Feedback

Both the climatological surface cloud radiative effect (CRE) and surface cloud feedback at the NSA site are calculated. The results of this analysis can be found in Sect. 3.2. We split the surface CRE by season so that the impacts of clouds in the Polar day, night, and transitional seasons can be seen clearly. The CRE was calculated using the kernels presented in Zhou et al. (2022) following the climatological CRE method formulated therein. The kernels were created using the Rapid Radiative Transfer Model (Mlawer et al., 1997) forced by observationally based input files generated via climatological average of relevant variables from 2000 to 2018 as reported by ERA-interim (Dee et al., 2011). Multiple sets of kernels are presented in Zhou et al. (2022): CTP and COD joint histograms of CF; and cloud base pressure (CBP) and COD joint histograms of CF

https://doi.org/10.5194/egusphere-2025-6553
Preprint. Discussion started: 8 January 2026

in both the LW and the SW. The CTP influences the TOA CRE far more than the CBP, and similarly for the surface CRE and CBP, hence the creation of both sets of kernels (Zhou et al., 2022). Kernels encoding the SW and LW CRE of liquid and ice clouds at the TOA and surface were generated for all latitudes, longitudes, and months of the year, and we subsequently use the surface kernels associated with the latitude and longitude box containing the NSA site. Our focus rests on the surface feedback based on the clouds in our dataset being limited to the column between the surface and 680 hPa and our observation of them using a surface based instrument.

We bin our data into joint histograms of CBP against COD. The CBP is determined by converting the ceilometer measured cloud base height into pressure values using the interpolated vertical atmospheric profiles created from radiosonde measurements discussed in Sect. 2.2. The value in each histogram bin is not the traditional cloud area fraction, as our dataset is based on a point observation. Rather, we count the number of successful quality controlled retrievals in each month and divide by the number of total converged retrievals prior to quality control. This gives a temporal CF representing the occurrence rate of low, stratiform, optically thin clouds in our dataset. We create two histograms for every month, calculating a liquid containing and an ice containing CF binned by CBP. These liquid and ice CBP histograms are then multiplied by their respective liquid or ice surface CRKs to produce a surface CRE for the liquid and ice components of all clouds in a given month.

We also calculate the surface based cloud feedback. To do so, CF anomaly histograms were created with the value in each histogram bin being the monthly CF after subtracting the climatological average CF for that month. In order to remove internal variability to isolate a coherent feedback signal we apply a low-pass filter to these CF anomaly histograms to damp signals of a period shorter than 10 years. This value was selected to isolate the signal with the highest power in the liquid CF anomaly time series (Fig. B1). A signal with relatively large power occurring on a 9 year period is seen which could represent the influence of low frequency oscillations such as the PDO, which can have a strong impact on Arctic cloud properties (Bi et al., 2021). We want to remove this signal from our cloud fraction anomaly time series before calculating the cloud feedback as this represents the influence of internal variability and will obscure the influence of global temperature changes on the temporal cloud fraction anomaly, which is the target of our cloud feedback analysis. Our low-pass filtering dampens this 9 year signal of internal variability as well as high frequency noise. After filtering, the resulting CF anomaly histograms were multiplied by the CBP kernels to generate the surface ΔCRE for both the SW and LW, as in

$$\Delta CRE = \frac{\partial R}{\partial C} \times \Delta C, \tag{3}$$

where $\frac{\partial R}{\partial C}$ is the cloud radiative kernel and ΔC represents the monthly anomalies of temporal cloud fraction binned by CBP and COD. These monthly cloud forced surface radiative anomalies are then averaged both annually and seasonally and regressed against both annually and seasonally averaged global surface temperature anomalies as in Gregory et al. (2004). The slope of these regression lines annually and in each season are considered the surface cloud feedback of low-level, single-layer, optically thin stratiform clouds at the NSA site.

https://doi.org/10.5194/egusphere-2025-6553
Preprint. Discussion started: 8 January 2026

2.3.2 Investigating Changes in Cloud Properties with Temperature

We use the methodology of Tan et al. (2019), which is an extension of Tseloudis et al. (1992), to diagnose the contributions to COD changes with temperature from phase shifts, liquid, and ice processes. The results of this analysis can be found in Sect. 3.3. In observations by the Moderate Resolution Imaging Spectroradiometer (MODIS) instrument, carried on the Terra and Aqua satellites, the COD in each 1° by 1° grid cell is decomposed into contributions from ice and liquid clouds, weighted by the normalized number of pixels in each grid cell covered by these ice and liquid clouds. This allows for the synthesis of information on distinct cloud phases into a single metric of the radiative impact of the COD. We perform a similar phase weighting process for the purposes of our analysis, but since our dataset is based on a single point observation rather than global satellite observations we weight by the fraction of the total water path (TWP) made up by the IWP and LWP respectively. Additionally, our dataset is averaged at a monthly level rather than at the daily time resolution.

We bin our data by the monthly average air temperature of the column extending from the surface to 680 hPa as determined by radiosonde, hereafter referenced as T_{low}. We use overlapping $15^\circ C$ wide bins, with bin centers separated by $1^\circ C$. For each bin, the derivative of the natural logarithm of COD with column averaged temperature is calculated according to Equation 5 of Tan et al. (2019),

$$\frac{d\overline{ln\tau}}{dT_{low}} = \frac{dk_i}{dT_{low}}\left(\overline{ln\tau_i} - \overline{ln\tau_l}\right) + k_i\frac{d\overline{ln\tau_i}}{dT_{low}} + k_l\frac{d\overline{ln\tau_l}}{dT_{low}}. \tag{4}$$

In Equation 4, k_i (k_l) is the monthly averaged normalized ice (liquid) water path, $ln(\tau_i)$ ($ln(\tau_l)$) is the monthly average of the natural logarithm of the ice (liquid) COD, and all derivatives are calculated as the slope of the regression line between the numerator and denominator in a given bin. The three terms on the right represent the contributions to the change in the COD from phase shifts, IWP mediated ice COD, and LWP mediated liquid COD respectively. Error bars are attached to each binned regression representing the 95% confidence interval of the regression slope based on a Student's t-test. To avoid exceedingly noisy regressions at the edges of the temperature distribution, we limited the bins included in the annual analysis to those for which there were 80 or more available months to regress over, while this limitation was relaxed in the seasonal analysis to bins including 40 or more months. While relaxing this criteria results in greater uncertainty, it is necessary to perform a seasonal decomposition as fewer points are available when considering only a single season.

To address how changes in different cloud properties may have contributed to these COD changes, we turn to the empirical relationship linking COD to the liquid water content (LWC), cloud physical thickness (CPT), and $r_{eff,liq}$ in liquid water clouds (Stephens, 1978):

$$\tau_l = \frac{3}{2}\frac{LWC \times CPT}{r_{eff,liq}}. \tag{5}$$

Taking the natural logarithm of Equation 5 and subsequently differentiating by temperature and multiplying by the monthly averaged normalized liquid water path allows for the decomposition of Term 3 of the right hand side (RHS) of Equation 4 directly:

https://doi.org/10.5194/egusphere-2025-6553
Preprint. Discussion started: 8 January 2026

$$k_l \frac{d\overline{ln\tau_l}}{dT_{low}} = k_l \frac{d\overline{ln(LWC)}}{dT_{low}} + k_l \frac{d\overline{ln(CPT)}}{dT_{low}} - k_l \frac{d(\overline{ln(r_{eff,liq})}}{dT_{low}}. \quad (6)$$

These derivatives are calculated via linear regression, with the overbar indicating monthly average. The CPT was calculated from a combination of micropulse lidar and cloud radar observations, considering only single layer stratiform clouds based on the definition in Terai et al. (2019). The details of the CPT derivation can be found in Stauffer et al. (2025), as we use the stratiform mask presented therein. The $r_{eff,liq}$ was retrieved by MIXCRA as per Sect 2.2. It should be noted that Equation 5 only applies to pure liquid clouds, and as such we only apply this decomposition to retrievals for which the ice COD was zero, and to only the liquid COD, LWC, and $r_{eff,liq}$ of mixed-phase retrievals. The results of this analysis can be found in Sect. 3.4.

2.3.3 Cloud Controlling Factor Analysis

To address how non-cloud properties, such as meteorological variables and aerosol concentrations which are considered cloud controlling factors (CCFs), may have contributed to COD changes, we perform a series of multiple linear regressions (MLRs), as in Ceppi and Nowack (2021); Klein et al. (2017); Myers et al. (2021); Naud et al. (2023), and Tan et al. (2024b). The results of this analysis can be found in Sect. 3.5. Observations of temperature, relative humidity, surface wind speed, and potential temperature (used to calculate lower tropospheric stability) are taken from various instruments at the NSA site, as per (Stauffer et al., 2025). Additionally to these observations, MERRA-2 reanalysis data are used to determine aerosol concentrations in the cloudy layer and vertical motion at the 500 hPa level (Global Modeling and Assimilation Office (GMAO), 2015). All observations have different units and magnitudes, and as such our MLR is performed using a standard score $s = \left(\frac{x-\overline{x}}{\sigma}\right)$, where x and $\overline{x}$ represent the monthly average and monthly climatological values of a particular variable respectively, and σ represents the standard deviation of the hourly observations averaged to produce the monthly values (Stauffer et al., 2025). Similar to the process outlined in Stauffer et al. (2025), we perform two regressions, one with all available CCF variables and one using a subset of those variables that maximizes the adjusted r^2 of their predictive power on the natural logarithm of the total COD.

2.3.4 Linear Trend Detection

We search for a statistically significant trend with time in our COD values at the 95% confidence level. The results of this analysis can be found in Sect. 3.6. This is done via the trend detection framework laid out in Liu et al. (2022), which is a weighted linear regression based off the work presented in Tiao et al. (1990) and Weatherhead et al. (1998). This calculates a trend using monthly COD values weighted by the intra-month variability in COD such that monthly averaged values based off of highly variable observations contribute less to the detected trend. Additionally, this method calculates the uncertainty in this trend using the MIXCRA retrieved uncertainty values in the COD. Using this trend magnitude and associated uncertainty, we can make conclusions on the significance of the detected linear trend at the 95% confidence level. Further details of the specific derivation of this trend detection framework and its capabilities can be found in Liu et al. (2022).

https://doi.org/10.5194/egusphere-2025-6553
Preprint. Discussion started: 8 January 2026

3 Results

3.1 Characteristics of the COD Dataset

We find that the liquid COD is climatologically greater than the ice COD in all months, with two maxima occurring in May and August (Fig. 1). This double peak occurs in most years (not shown). The ice COD is relatively constant for most of the year but reduces to near 0 values in the summer. We also find that the majority of clouds recorded in our dataset are purely liquid water (Tab. 1). These account for 70.0% of the total recorded clouds, with another 29.8% being mixed-phase, with both an ice and liquid COD recorded. Our observation of close to 30% of all low-level, stratiform, single layer clouds above the NSA site being mixed-phase in the annual average aligns well with a previous analysis that includes data from a high spectral resolution lidar and a Ka-band radar (Zhang et al., 2019). A very small 0.2% of the clouds in our dataset are of pure ice phase. Mixed-phase clouds are the dominant phase in winter, liquid clouds are dominant in summer, and there is a nearly equal occurrence of liquid and mixed-phase clouds in spring and autumn (Tab. 1). Seasonally, our analysis also generally agrees with Zhang et al. (2019) in the spring and summer with close to 50% and 20% of all clouds being mixed-phase respectively. In the winter and autumn, our analysis indicates a larger percentage of all clouds being mixed-phase than Zhang et al. (2019). Ice clouds do not exceed 2% in any season.

This lack of pure ice clouds is due to a combination of multiple factors. Supercooled liquid is commonplace in Arctic clouds and mixed-phase clouds containing supercooled liquid do not immediately glaciate, often remaining in this mixed phase state for long periods of time (Morrison et al., 2012; Korolev et al., 2017; Mioche et al., 2017). It has also been shown that temperature is the dominant control on cloud phase, with mixed-phase clouds being observed frequently even at cold temperatures relatively close to the threshold for homogeneous freezing of liquid water (Tan et al., 2014). Additionally, our dataset inherently represents warmer clouds as the CTP is required to be lower than 680 hPa. Finally, our dataset, despite having observations during both summer and winter, is dominated by summer observations, during which the occurrence of ice-phase clouds is less than 0.5% (Tab. 1). This summertime bias, as seen in Fig. 2, is primarily due to the requirement that the uncertainty in the COD is less than 15% of the COD itself (not shown). This results in the removal of far more wintertime than summertime retrievals, as the ice COD is typically smaller than the liquid COD (Fig. 1) and as such the ratio of the uncertainty to the total COD will be larger in the winter due to more ice, hence smaller COD values. A modification of this 15% uncertainty threshold for small COD would result in the inclusion of more wintertime points, but would represent a decrease in the accuracy of the reported COD values.

3.2 Climatological Cloud Radiative Effect and Cloud Feedback

The presence of low, stratiform clouds over the NSA site results, in the climatological average, in increased surface absorption of radiation as compared to clear sky conditions due to stronger LW emission than SW reflection (Fig. 3). The LW CRE remains relatively constant throughout the seasons, resulting in the net surface CRE being greatest in the winter where the SW CRE is nearly non-existent, and near zero in the summer where the SW CRE is large. While it may initially seem counterintuitive that clouds do not produce a strong surface radiative deficit in the summer when the SW effect is expected to dominate (Curry

https://doi.org/10.5194/egusphere-2025-6553
Preprint. Discussion started: 8 January 2026

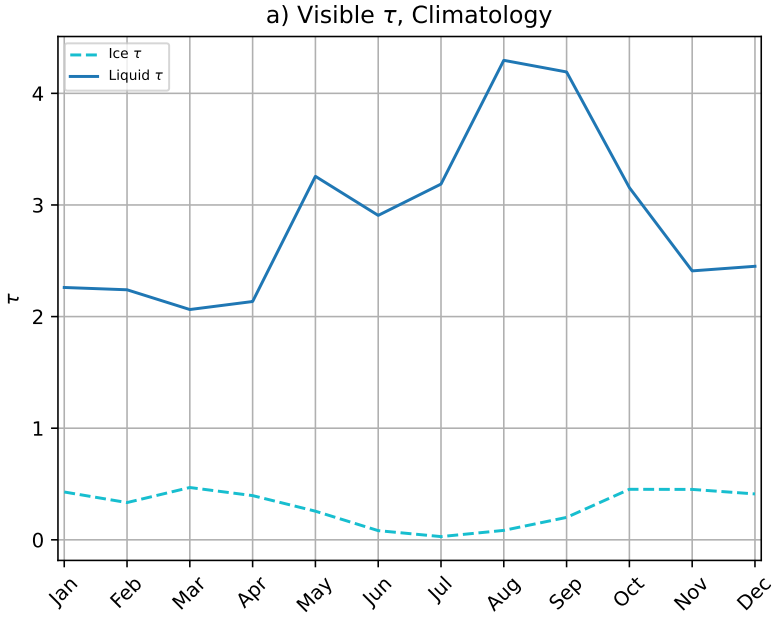

Figure 1. Climatology of the visible liquid and ice COD of low-level, single-layer, optically thin stratiform clouds from April 2002 to August 2023 over the NSA site as retrieved by the MIXCRA algorithm.

Table 1. Annual and seasonal summary of the phases of all observed clouds in the dataset, with pure ice (liquid) clouds defined as any cloud with 0 reported liquid (ice) COD. Mixed phase clouds are any clouds with both ice and liquid COD being non-zero.

	Pure Liquid Phase	Pure Ice Phase	Mixed Phasee
Annual	70%	0.2%	29.8%
Winter	35.4%	1.9%	62.7%
Spring	44.8%	0.8%	54.4%
Summer	79.0%	0.0%	21.0%
Autumn	51.1%	0.2%	48.7%

https://doi.org/10.5194/egusphere-2025-6553
Preprint. Discussion started: 8 January 2026

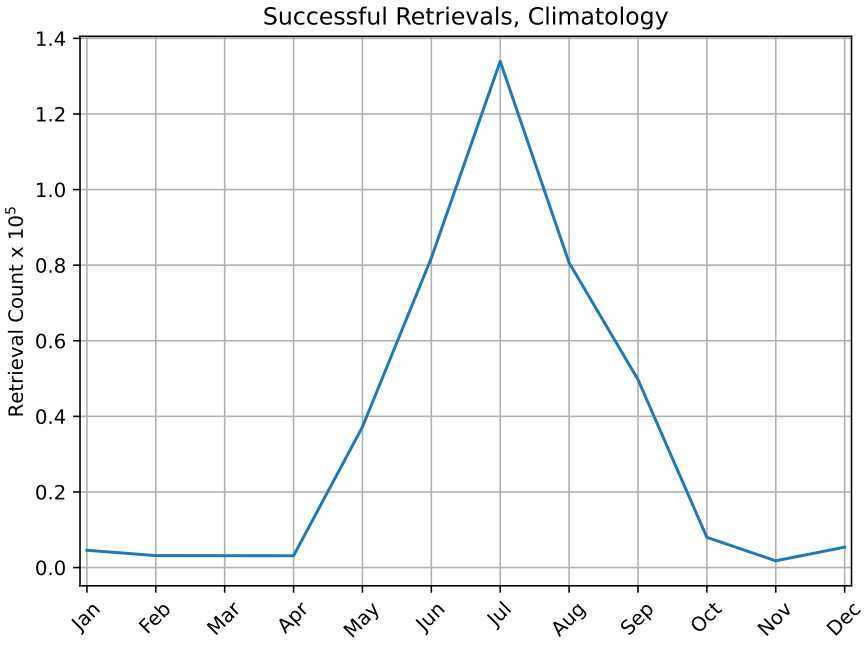

Figure 2. Climatology of the completed retrievals of the MIXCRA algorithm, after quality control limitations have been applied. The y-axis includes a factor of 10^5 and represents the average number of successful retrievals in a given month.

et al., 1996; Allan, 2011), our result is due to the subset of the total clouds that we have chosen to study. We specifically focus on low, stratiform, optically thin clouds to cater to the strengths of the MIXCRA algorithm, and as such the negative SW CRE of these clouds is relatively small when compared to optically thicker clouds. The LWP of clouds in our dataset is generally much lower than the LWP of all clouds over the NSA site, as can be seen in empirical cumulative distribution functions of our MIXCRA retrieved LWP and the LWP as measured by a collocated microwave radiometer (Fig. C1). Additionally, the LWP of clouds in our dataset is generally lower than the LWP of similarly single-layer, stratiform clouds as measured by MWR and reported in Zhang et al. (2019), although this is expected given the use of the MWR in their study, and direct comparison is not easy given their focus on exclusively mixed-phase clouds while we also consider ice and liquid clouds.

Concurrent cloud fraction and cloud optical depth changes in our dataset result in a negative cloud feedback over the 21 years that we analyze; with a negative feedback seen annually and in every season except the summer (Fig. 4). The feedback is most negative in the winter and autumn, and most positive in the summer where a large and positive SW liquid feedback offsets the negative LW liquid feedback. The signs of the individual feedback components indicate that clouds over the NSA site are either optically thinning or becoming less frequent (a reduced temporal cloud fraction), allowing more SW radiation to be absorbed by the surface and emitting less LW radiation. We do not consider influences of CBP changes as our data are limited to clouds with CTP below 680 hPa. This means that all of our clouds fall into the lowest two CBP bins and the majority are in the lowest bin (not shown). Of the two competing influences of increased surface SW absorption and decreased LW

https://doi.org/10.5194/egusphere-2025-6553
Preprint. Discussion started: 8 January 2026

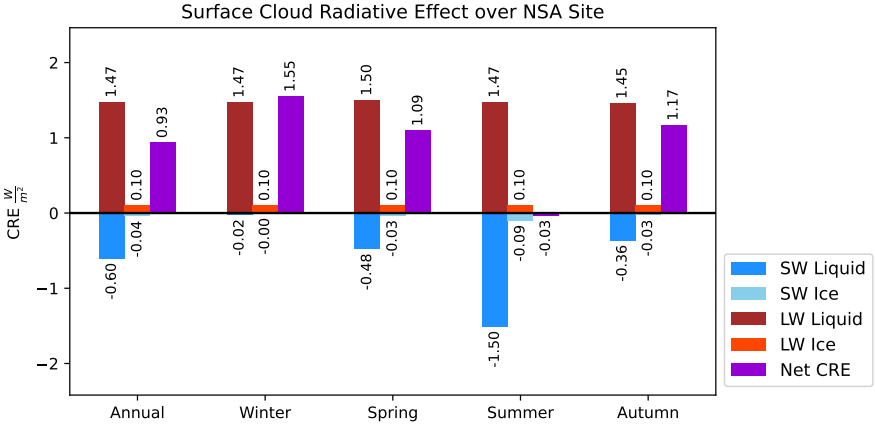

Figure 3. Climatology of the surface CRE in Wm^{-2} calculated via a temporal cloud fraction and observational cloud radiative kernels. Individual seasonal CRE values appear at the end of each bar, and the Net CRE is calculated as the sum of the individual SW and LW liquid and ice surface CREs.

emission to the surface by clouds, the decreasing LW emissions dominate in every season other than summer, as evidenced by the negative sign of the net cloud feedback. Generally, the r^2 values of the seasonal and annual regressions are low (Tab. D1) and as such none of the feedbacks are statistically significantly different than 0 at the 95 % confidence level, except for the LW liquid feedback in autumn. This indicates that much of the variance in the cloud induced surface radiative anomaly, even after smoothing, can be explained by factors other than globally averaged surface temperature. In the same vein, the values of Fig. 4 should not necessarily be considered representative of the long-term Arctic cloud feedback as it is only a two decade long trend. Nevertheless, it is important to consider how cloud changes, as mediated by global surface temperature trends, are impacting the radiative budget at the Arctic surface especially in the context of Arctic amplified warming and anthropogenic climate change.

3.3 Change in the Cloud Optical Depth with Temperature

Throughout the entire year clouds existing in the lower-troposphere with average temperature near $0°C$ become optically thinner with warming, while clouds existing in a colder ($< -4°C$) atmosphere either show no change or become thicker with warming (Fig. 5). The shape and magnitude of this curve agrees with previous observational analyses of Arctic COD changes with temperature at the NSA site (Terai et al., 2019). Additionally, while the magnitude differs slightly, the shape of our curve agrees with previous observational analyses considering data outside of the Arctic, (Tseloudis et al., 1992; Tan et al., 2019), as well as CMIP3 and CMIP5 model analyses which do consider the Arctic (Gordon and Klein, 2014). A seasonal decomposition is overlaid on the annual curve. This decomposition shows that summertime clouds, which primarily exist in a near $0°C$ column averaged temperature, decrease in COD with warming. Spring and autumn clouds, which typically have column averaged temperatures between $-5°C$ and $-15°C$ increase in COD with warming. Wintertime clouds, typically in a

https://doi.org/10.5194/egusphere-2025-6553
Preprint. Discussion started: 8 January 2026

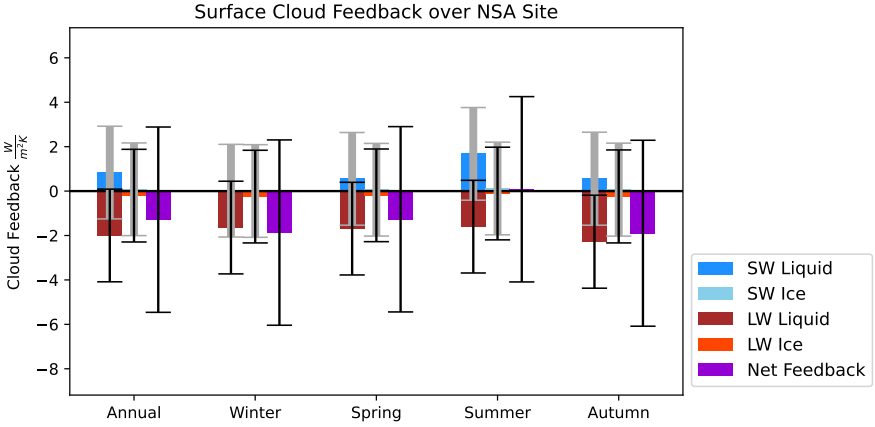

Figure 4. The cloud feedback over the NSA site in $Wm^{-2}K^{-1}$ calculated via temporal cloud fraction and observational cloud radiative kernels. As in Fig. 3, the Net Feedback is calculated as the sum of the individual SW and LW liquid and ice surface cloud feedbacks. The error bars represent the 95 % confidence interval of the Gregory regression used to calculate the feedback value, with the thicker, grey error bars being associated with the SW feedbacks, and the thinner, black error bars being associated with the LW feedbacks. The Net feedback error bars were calculated by adding the individual feedback error bars in quadrature. Feedback values and the r^2 values of each regressions are collected in Tab. D1.

column averaged temperature $< -15°C$, decrease in COD with warming. This agrees with the sign of the winter surface cloud feedback in Fig. 4. Monthly averaged WP weighted $dln(\tau_{low})/dT_{low}$ values exist in each season at temperatures both warmer and colder than the ends of their respective curves in Fig. 5, but the 40 month minimum requirement to report a bin precludes visualization of these points. There is some overlap between the seasons, particularly from spring and autumn monthly points occurring at colder temperatures than $-15°C$. This can be seen in the large uncertainty in COD changes for clouds in column averaged temperatures $< -15°C$ in the annual curve as there are competing influences from multiple seasons.

Changes in the LWP mediated liquid COD with temperature (Term 3 of the RHS of Equation 4) are the largest contributors to the overall shape of the curve in Fig. 5, with phase shifts (Term 1 of the RHS of Equation 4) being the next largest contributor (Fig. 6). Changes in the IWP mediated ice COD (Term 2 of the RHS of Equation 4), while considering relatively large error bars, contribute very little. In column average temperatures $< -5°C$, increasing LWP mediated liquid COD and a positive phase shift term result in a large increase in COD with warming. In column average temperatures near $0°C$, decreasing LWP mediated liquid COD is slightly offset by a positive phase shift term, resulting in an overall decrease in the COD. The phase shift term contributes to changes in the COD with warming even at relatively warm temperatures, in part due to the 21 % of summertime clouds observed to be mixed-phase (Tab. 1). The sum of the liquid, ice, and phase shift curves is shown in black in Fig. 6, and it agrees well, especially considering the envelope produced by the error bars, with the annual curve in Fig. 5.

https://doi.org/10.5194/egusphere-2025-6553
Preprint. Discussion started: 8 January 2026

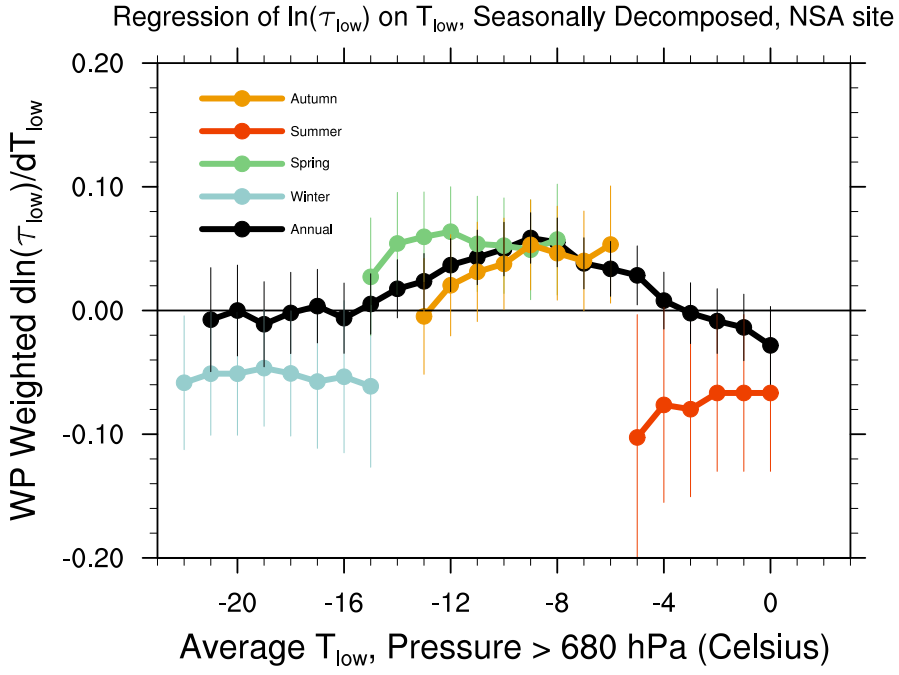

Figure 5. Regression of the monthly averaged natural logarithm of the COD against the monthly averaged temperature of the atmospheric column from the surface to 680 hPa using retrievals from each season overlaid on a curve using retrievals from all seasons combined. The y-value of each point represents the regression slope of a $15°C$ wide bin centered on the x-value of the point. Error bars represent the 95 % confidence interval of the regression. Regression slopes making up the annual curve are only reported for bins that contain 80 or more points, while regression slopes making up the curves for each season are reported for bins that contain 40 or more points. Cyan points represent winter COD changes, green points represent spring COD changes, orange points represent autumn COD changes, and red points represent summer COD changes.

3.4 Change in the Liquid Water Content, Cloud Physical Thickness, and Liquid Effective Radius with Temperature

The LWC of clouds in our dataset generally increases with warming except at temperatures below $-16°C$ and in the summer season (Fig. 7a). Additionally, the CPT of clouds in our dataset decreases with warming at all temperatures greater than $-11°C$ (Fig. 7b). This suggests that increases in COD with warming seen at temperatures between $-16°C$ and $-4°C$ (Fig. 5) are due to increases in LWC with warming. Additionally, decreasing COD with warming at near $0°C$ temperatures and in the entire summer season are due to decreases in the CPT with warming. In the summer season this combines with decreases in LWC with warming. Small but statistically significant increases in $r_{eff,liq}$ are seen annually and in the spring and autumn (Fig. 7c). While these changes are small, it is necessary to include them to achieve closure of the decomposition presented in Equation 6, which is demonstrated by the match between Fig. 7d, which is a reproduction of the liquid term from Fig. 6, and Fig. 7e, which is the sum of Fig. 7a and Fig. 7b, minus Fig. 7c.

https://doi.org/10.5194/egusphere-2025-6553
Preprint. Discussion started: 8 January 2026

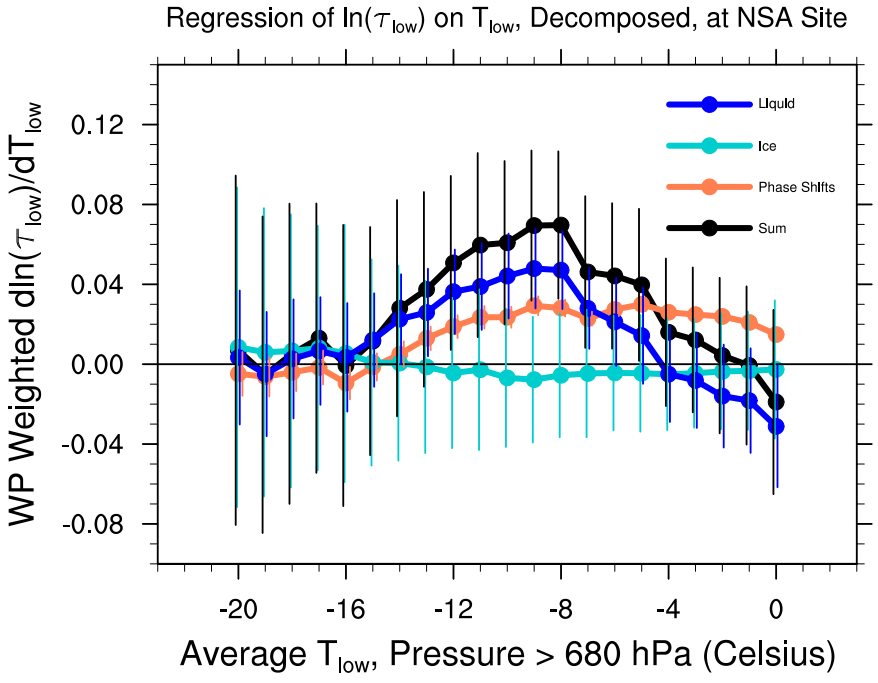

Figure 6. Decomposition of Fig. 5 according to the three terms of the RHS of Eq. 4. The orange curve represents phase change processes, or the first term on the RHS of Eq. 4. The cyan curve represents the second term of the RHS of Eq. 4. The blue curve represents the third term of the RHS of Eq. 4. The y-value of each point represents the regression slope of a $15°C$ wide bin centered on the x-value of the point. Error bars represent the 95 % confidence interval of the regression in each decomposed term, while the error bars of the liquid, ice and phase shift terms are added in quadrature to produce the error bars on the summed curve. Regression slopes are only reported for bins that contain 80 or more points. Error bars have been slightly offset from one another to avoid overlap.

The shapes and magnitudes of the annual curves in Fig. 7a and 7b agree well with the model based analysis of Fig. 2 of Gordon and Klein (2014). Decreasing CPT with warming at all temperatures above $-11°C$ could be due to increases in precipitation efficiency of liquid particles due to their larger size at warmer temperatures, or it could possibly be the result of entrainment of dry air. This result is broadly consistent with model based studies of boundary layer stratocumulus clouds such as Bretherton and Wyant (1997) and Blossey et al. (2013), despite the fact that they do not focus on the Arctic. A precipitation efficiency based argument could align with the observed decrease in the liquid COD with warming and the slightly less positive values of the phase shift term at temperatures above $-4°C$ in Fig. 6. It should be noted that Fig. 2 of Gordon and Klein (2014) and Fig. 7 should not be considered for direct comparison as Figure 2 of Gordon and Klein (2014) was created by grouping model output at all latitudes while Fig. 7 only uses observations taken at a single point location. Despite our use of a point observation and their grouping of all latitudes, the agreement we see with Gordon and Klein (2014) is encouraging and suggests that model ensemble representations of the relationship between CWC and CPT changes and COD

https://doi.org/10.5194/egusphere-2025-6553
Preprint. Discussion started: 8 January 2026

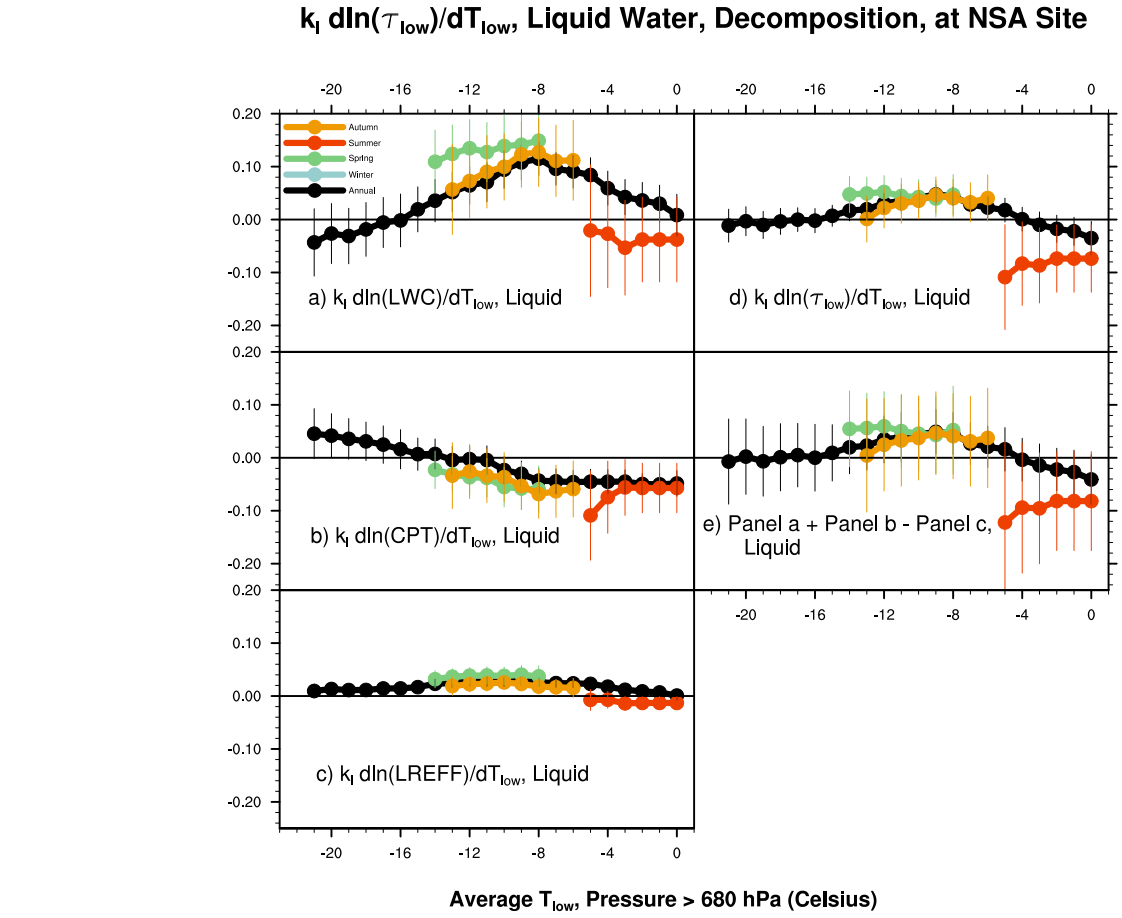

Figure 7. Regression of the monthly averaged natural logarithm of the a) LWC of liquid and mixed phase clouds, b) CPT of liquid and mixed phase clouds, and c) $r_{eff,liq}$ of liquid and mixed phase clouds against the monthly averaged temperature of the atmospheric column from the surface to 680 hPa, decomposed seasonally. The y-value of each point represents the regression slope of a $15^{\circ}C$ wide bin centered on the x-value of the point. Error bars represent the 95 % confidence interval of the regression. Panel d) is a reproduction of the Liquid curve from Fig. 6, and e) is panel c) subtracted from the sum of panel a) and panel b). Panels d) and e) are included to demonstrate the closure achieved by Equation 6. Regression slopes are only reported for bins that contain 80 or more points for the annual curves, and 30 or more points for the seasonal curves. No points are reported for the winter season as there were not more than 30 points in any bin.

https://doi.org/10.5194/egusphere-2025-6553
Preprint. Discussion started: 8 January 2026

may be representing observational results well, and that the NSA site could be representative of these physical relationships in most of the Arctic region as a whole.

3.5 Change in the Cloud Optical Depth with non-Cloud Properties

The column averaged atmospheric temperature is not the only environmental variable that controls the COD. Changes in other properties of the atmosphere over the NSA site can impact the COD, and investigation of these impacts is important to better our understanding of the Arctic COD and its controls. Fig. 8a shows the sensitivity of the natural logarithm of the COD of low-level, single-layer, optically thin, stratiform clouds to a series of CCFs observed at the NSA site. These CCFs are the temperature at the 850 hPa level (Ta_{850}); the relative humidity averaged over the surface, 850 hPa, and 700 hPa levels ($RH_{avg,col}$); the surface wind speed (u_{sfc}); the lower tropospheric stability (LTS); the subsidence at the 500 hPa level (ω_{500}); and the sea salt (SS), dust (DU), hydrophilic black carbon (BCPHILIC), hydrophilic organic carbon (OCPHILIC), sulfur dioxide (SO_2) and sulfate (SO_4) concentrations averaged over the cloudy layer as described in Stauffer et al. (2025). The first five variables represent meteorological conditions expected to impact COD (Myers et al., 2021), while the final five represent aerosol species expected to be relevant to the COD (Stauffer et al., 2025). Fig. 8a represents the full multiple linear regression using every single CCF so that the sensitivity of the natural logarithm of the COD to all CCFs can be seen. Following the analytic framework presented in Stauffer et al. (2025) we perform a second MLR that maximizes the predictive power of these CCFs on the COD. This means that our MLR was iteratively run with every possible subset of our chosen CCFs until the specific subset maximizing the r^2 value of our regression is found. This can be seen in Fig 8b, with the r^2 value of 0.516 indicating that a hypothetical model for the COD using the Ta_{850}; u_{sfc}; and sea salt, OCPHILIC, and SO_2 concentrations would be able to explain 51.6 % of the variance in the COD at the NSA site (Fig. 8b). This represents the maximum variance in the COD that can be explained by any combination of the chosen CCFs.

It is expected that the significance and magnitude of the sensitivity of changes in the natural logarithm of COD to changes in the individual CCFs will change between the original (Fig. 8a) and optimized (Fig. 8b) regressions as the optimization does not represent a simple selection of bars from Fig. 8a, but rather a repetition of the MLR using only a subset of the CCFs. We select the column averaged RH as a CCF rather than the RH at a single level as we do not expect anomalously high monthly averaged RH at a single level to imply anomalously high monthly averaged COD from a point observation. Stauffer et al. (2025) use the RH as a CCF because their predicted variable, stratiform CF, is derived as a temporal CF and as such months for which the average RH at a single level is anomalously high represent more frequent RH saturations and cloud formation, implying a higher temporal CF (Fig. 3a of Stauffer et al. (2025)). Other MLRs (Myers et al., 2021; Ceppi and Nowack, 2021) consider grid box averaged values, for which a higher monthly average RH would also imply a higher area CF. The same logic does not apply to our COD, which is not based off a frequency or spatial measurement, and is rather the sampling of a cloud property at a single point. The use of a column averaged RH therefore represents the increase of the RH in the cloudy environment that we are observing and as such is more applicable to the COD of a single layer, thin cloud. It should be noted that any agreement or disagreement between this paper and Stauffer et al. (2025) must be considered in the context that each manuscript investigates

https://doi.org/10.5194/egusphere-2025-6553
Preprint. Discussion started: 8 January 2026

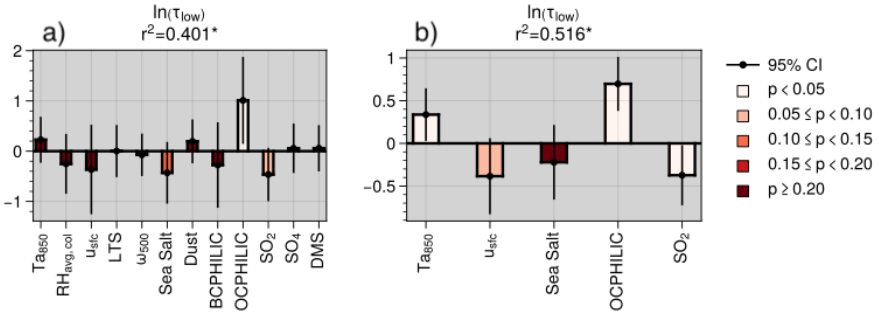

Figure 8. Multiple linear regression of the natural logarithm of total COD against a) all chosen CCFs and b) a subset of chosen CCFs that maximizes the predictive power of the CCFs on the natural logarithm of the total COD. The magnitude of each bar represents the sensitivity of changes in the natural logarithm of the COD to changes in the indicated CCF, while the sign indicates the nature of this relationship. The shading of each bar represents the statistical significance of the covariance between the CCF and the natural logarithm of the total COD. All CCFs and the natural logarithm of total COD are normalized anomalies from the monthly mean. Error bars indicate the 95% confidence interval of the regression.

distinct cloud properties which are both important to the radiative characteristics of the NSA site but ultimately dissimilar: the CF and the COD.

Of all CCFs, the natural logarithm of the total COD is most sensitive to changes in concentration of OCPHILIC (Fig. 8). This is a large, statistically significant at the 95% confidence level, and positive relationship such that increases in OCPHILIC occur at the same time as increases in COD. This may be due to the efficiency of OCPHILIC as a CCN (Sun and Ariya, 2006), such that increases in OCPHILIC will result in more liquid cloud particles, which for the same amount of cloud water will increase the COD. Additionally, if there is a concurrent increase in cloud water, anomalously high OCPHILIC levels provide an avenue for increased LWP. Both of these processes would result in positive changes in COD (Fig. 6). A statistically significant and negative relationship between SO_2 and COD also exists in the optimized MLR (Fig. 8b). This agrees with the negative relationships between SO_2 and both CF and LWP found in Stauffer et al. (2025). In that paper this relationship is posited to be a consequence of oxidation of SO_2 into SO_4 within clouds, with SO_4 being an efficient CCN but inhibiting ice nucleation on INPS (Kanji et al., 2017). Therefore an increase in COD would be concurrent with a decrease in SO_2, although the lack of a statistically significant relationship between COD and SO_4 indicates that the CCN mediated influence of SO_4 on COD may be minimal.

A positive statistically significant relationship between Ta_{850} and COD in our optimized MLR supports the positive relationship between COD and the average temperature of the low atmospheric column at most temperatures seen throughout this manuscript (Figs. 5, 6, 7). A negative relationship between u_{sfc} and COD is seen in our optimized model. While previous literature has found a positive relationship between surface wind speed and both marine low-cloud cover (Qu et al., 2015; McCoy et al., 2017) and the COD over the Southern Ocean (Tan et al., 2024a), these results are presented as being mainly due to surface wind speed resulting in increased evaporation and positive flux of water vapor into the boundary layer. In our

https://doi.org/10.5194/egusphere-2025-6553
Preprint. Discussion started: 8 January 2026

dataset this effect would be dependent on the wind direction considering that the NSA site is a coastal station and frequent sea-ice decouples the cloudy layer from this local source of water vapor, although sea-ice cover is not year-round. It has been posited that a negative relationship between the surface wind speed and COD is possible due to increased lofting of INPs (Tan et al., 2024a), which would decrease the droplet number concentration and therefore the COD of the clouds above the NSA site, which would explain the negative relationship seen here. This impact could be amplified at the NSA site given the relatively pristine nature of the Arctic atmosphere. This could also be reflected in the negative relationship between sea salt concentrations and the natural logarithm of the COD seen in our optimized MLR, but a clear analysis of this relationship is precluded by a low correlation and large error.

In our non-optimized, full MLR, there exists a highly uncertain but potentially negative relationship between the natural logarithm of the COD and the column averaged relative humidity. This is counterintuitive, as it is expected that increasing column averaged RH would represent the deepening of the cloud layer and as such increasing COD. The observed negative relationship is supported by the results of Stauffer et al. (2025), which indicates a positive relationship between the RH and both IWP and median particle size, and a negative relationship between the RH and supercooled liquid fraction. This implies that increasing RH results in more cloud ice, larger cloud particles, and less supercooled liquid in mixed-phase clouds. These changes would result in an overall decrease in COD with increasing RH, as larger, less reflective ice particles have a lower COD than smaller, more reflective liquid particles for a given CWC.

3.6 Linear Trend

In addition to investigations of how the COD changes with temperature in our dataset, we employ the trend detection framework of Liu et al. (2022) to elucidate how the COD changes with time in our dataset. We seek statistically significant trends at the 95% confidence level in the total, ice, and liquid COD, the natural logarithms of the ice and liquid COD, and in the water path weighted natural logarithm of COD as in Eq. 4 (equivalent to $ln(\tau_l + \tau_i)$, (Tan et al., 2019)). Positive trends in the liquid (0.0719 year^{-1}) and total (0.0824 year^{-1}) COD were found to be statistically significant at the 95 % confidence level. These trends were plotted in Fig. 9 against the liquid and total COD timeseries after seasonal variability and background noise were removed from this data, according to the transformed linear model outlined in equation A6 of appendix A2 of Liu et al. (2022). It is expected that these two plots are similar to one another due to the relatively larger liquid COD detected in our dataset as compared to the ice COD, resulting in the liquid COD being the dominant influence on total COD. While this linear trend is statistically significant at the 95% confidence level, it is not expected to explain all of the variance in the COD. It is intended rather to give a sense of how the COD is changing over large time scales, and deviations from this trend are expected. It should also be noted that the trend detection framework takes into account intra-month variability in COD measurements, with highly variable months contributing less to the linear trend. The intra-month variability is not displayed in the timeseries of Fig. 9.

https://doi.org/10.5194/egusphere-2025-6553
Preprint. Discussion started: 8 January 2026

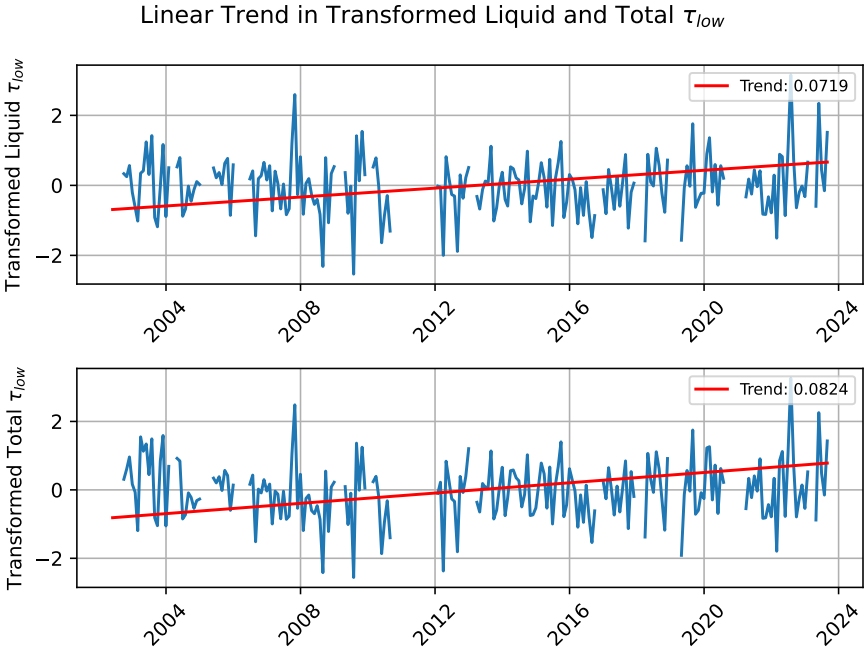

Figure 9. Detected linear trends in the liquid and total COD plotted over the liquid and total COD after transformation according to equation A6 of Liu et al. (2022) transformed liquid and total COD respectively.

4 Conclusions

We develop and analyze a 21 year dataset of cloud properties over the Department of Energy's North Slope of Alaska Atmospheric Radiation Measurement site, finding that clouds with temperatures between $-16°C$ and $-4°C$ in the lower troposphere become optically thicker with warming while clouds existing in environments warmer than $-4°C$ become thinner with warming, with little change observed at temperatures below $-16°C$. Both the optical thickening and thinning are driven by changes in cloud properties associated with the liquid phase, with thickening occurring primarily due to increases in LWC while thinning being driven by decreasing CPT. These results align with previous observational analyses of the NSA site (Terai et al., 2019) indicating that their findings, based on data from 2004 and 2005, are likely representative of the longer term relationships between clouds and temperature observed over Utqiagvik. Additionally, our results are in general qualitative agreement with the conclusions of a GCM study of changing COD with temperature (Gordon and Klein, 2014), indicating that models could be capturing the observed relationships between cloud properties and temperature well, and implying that the NSA site could be representative of the Arctic atmosphere as a whole.

The influence of a range of meteorological variables and aerosol concentrations on the COD are investigated. A statistically significant positive relationship between COD and OCPHILIC as well as a statistically significant negative relationship between COD and SO_2 are found, indicating that aerosol cloud interactions have strong yet competing influences on the COD above

https://doi.org/10.5194/egusphere-2025-6553
Preprint. Discussion started: 8 January 2026

the NSA site. In a given cloud, the interaction between aerosol concentration and COD likely depends on the phase distribution of the cloud, given the different abilities of OCPHILIC and SO_2 to act as CCN or INP. A positive relationship between COD and temperature at the 850 hPa level is also observed in the optimized MLR in 8b. This aligns with the positive slopes seen at most temperatures in Figures 5 and 6. This agreement must be considered in the context that the MLR uses temperature at the 850 hPa level while Figure 5 and 6 use the column averaged temperature of the layer between the surface and 680 hPa.

Figures 5 and 6 indicate that the COD of low-stratiform, optically thin clouds with small LWP values (Fig. C1) can either increase or decrease with warming based on the temperature of the cloud. Figure 8 shows an overall positive relationship between COD and atmospheric temperature at the 850 hPa level. Figure 9 shows an overall positive trend in the COD over the period of this analysis. Taken together, these results imply that COD increases at column averaged temperatures $< -5°C$ dominate COD decreases at near $0°C$ temperatures during the 21 years of our study. Additionally, while the CCF analysis is based on regression against local temperature and the linear trend analysis is based off of a regression against time and not globally averaged temperature, these findings suggest that the negative liquid LW feedbacks and positive SW feedbacks seen in all seasons apart from summer (Fig. 4) are driven more by decreasing cloud fraction than by changes in the COD. This is because optical thickening with warming and time, as suggested by Figures 5, 6, 8, and 9, would result in a positive LW and negative SW feedback. This means that the observed annual cloud feedback of low-level, single-layer, stratiform, optically thin clouds described in Fig. 4 must be caused by decreasing temporal cloud fraction.

Seasonal decompositions performed throughout the paper, however, indicate that the negative feedback seen in the winter season could be caused by either decreasing temporal cloud fraction or decreasing COD. This is because of the statistically significant decreases in the COD in winter at all temperatures (Fig. 5). Optical thinning with increasing temperature, particularly in the winter months when the SW impact of this thinning is minimal, would result in a negative LW feedback as less emission to the surface is occurring with warming. We were not able to make conclusions about the underlying causes of wintertime decreases in COD with temperature, as the lack of winter-time retrievals in our dataset precluded inclusion of this season in Fig. 7. The relatively low r^2 provided by the optimized MLR as seen in Fig. 8b indicates that while meteorological variables and aerosol concentrations are able to explain just over 50 % of the variance in the natural logarithm of the COD, there are other significant controls that are not captured by this analysis. Similarly, the low r^2 values of the cloud feedback regressions (Tab. D1) imply that globally averaged surface temperatures are not a dominant control on cloud properties over the NSA site. Many different variables exert strong influence on Arctic cloud properties and therefore the relationships between these variables and cloud properties must be considered holistically to fully explain observed changes in Arctic clouds.

Our results add credence to existing conclusions about the relationship between COD and temperature in the Arctic atmosphere. Additionally, we further investigate this relationship above the NSA site and expand our understanding of the many controls on cloud properties that exist in the Arctic atmosphere. There are limitations to this analysis, such as the lack of winter retrievals and the strong bias towards liquid and mixed-phase clouds. Additionally, the AERI instrument and MIXCRA algorithm impose on our study a focus on low-stratiform, optically thin clouds. While changes in these clouds are important to the surface flux balance (Fig. A1), we are limited in the scope of our conclusions. We also only analyze data from the NSA site. A future analysis could convolve information from multiple instruments and observational sites to potentially expand upon these

https://doi.org/10.5194/egusphere-2025-6553
Preprint. Discussion started: 8 January 2026

results and assess their validity over a longer temporal range and with more certainty about processes occurring in the Polar night.

State of the art climate models disagree about the sign and magnitude of the Arctic cloud feedback, and therefore AA. Our results imply that changes in low-stratiform, single-layer, optically thin clouds over the NSA site during the period from 2002 to 2023 act to decrease Arctic amplified warming. Decreasing cloud fraction results in a larger reduction in LW emission to the surface than increase in SW absorption. This impact, as mediated by global surface temperature, counteracts positive influences on AA such as the albedo and lapse rate feedbacks, thereby limiting AA. We do not make conclusions about the TOA cloud feedback given the subset of the clouds we are studying and the ground-based instrument we are observing them with. However, we provide evidence for a more negative surface Arctic cloud feedback at the NSA site due to changes in low-stratiform, single-layer, optically thin clouds. This manuscript and associated dataset represent the extension of an existing source of cloud microphysical properties to a temporal scale associated with climate processes. The role of cloud microphysics in the long-term Arctic cloud feedback, particularly in the context of the cloud phase feedback, is the source of much disagreement between climate models. Our analyses, and the dataset we present, can serve as an avenue for the evaluation and improvement of model representations of Arctic cloud microphysical processes. This will allow for further investigation of these processes and their impacts on the Arctic cloud feedback, Arctic Amplification, and global climate change.

Data availability. All cloud properties discussed here as well as necessary variables for quality control can be found published online at 10.5281/zenodo.17833181

Appendix A: Sensitivity of top of the atmosphere and surface fluxes to changes in cloud liquid water path

Our focus is on clouds with relatively small liquid water path (LWP) and cloud optical depth (COD). To demonstrate the importance of these clouds to the balance of flux at the top of the atmosphere (TOA) and surface in polar regions, plots of TOA and surface flux as a function of LWP (and therefore COD for set values of liquid particle effective radius) were generated, similar to Fig. SB1 of Turner et al. (2007). Rather than investigate the standard midlatitude profiles of Anderson et al. (1986) as was done in Turner et al. (2007), we use the standard subarctic atmosphere for the summer. These plots were made using the Rapid Radiative Transfer Model (Mlawer et al., 1997). For these calculations, an overcast cloud was placed at 2 kilometers above the surface, the sun was assumed to be directly overhead, and a value for the surface albedo of 0.1 was assumed. COD as a function of LWP was calculated via the empirical relationship defined in Stephens (1994).

Appendix B: Filtering of liquid temporal cloud fraction anomalies

The temporal cloud fraction anomalies seen in our dataset are used to calculate a cloud feedback. However, many signals of varying power and period can be found in this timeseries, and as such careful filtering must be performed to extract a coherent climate change signal for our feedback analysis. This timseries can be see in Fig. B1a, with the power spectra decomposition

https://doi.org/10.5194/egusphere-2025-6553
Preprint. Discussion started: 8 January 2026

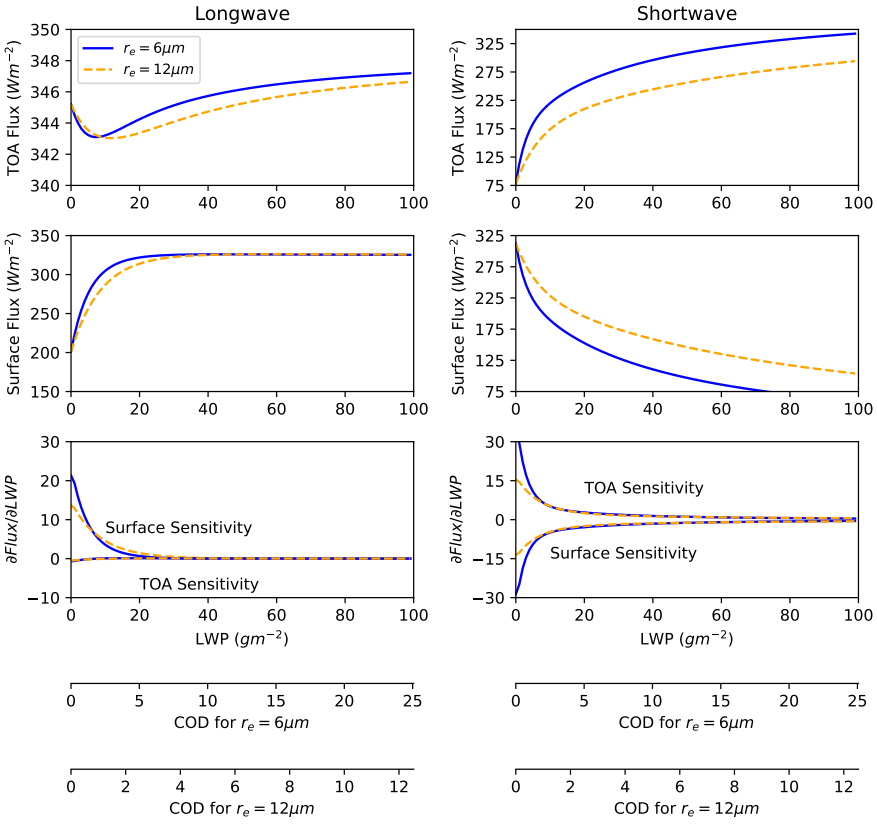

Figure A1. Top of the atmosphere and surface longwave and shortwave flux sensitivities to changes in cloud LWP and COD, as calculated using the Rapid Radiative Transfer Model and the U.S Standard Sub-polar atmosphere for the summer. An overcast cloud was placed 2 kilometers above the surface, the sun was assumed to be directly overhead, and a value for the surface albedo of 0.1 was assumed. Multiple secondary axes are provided to indicate the COD of a cloud with the given LWP for various effective radii, as calculated via the empirical relationship between water path, COD, and effective radius (Stephens, 1994).

https://doi.org/10.5194/egusphere-2025-6553
Preprint. Discussion started: 8 January 2026

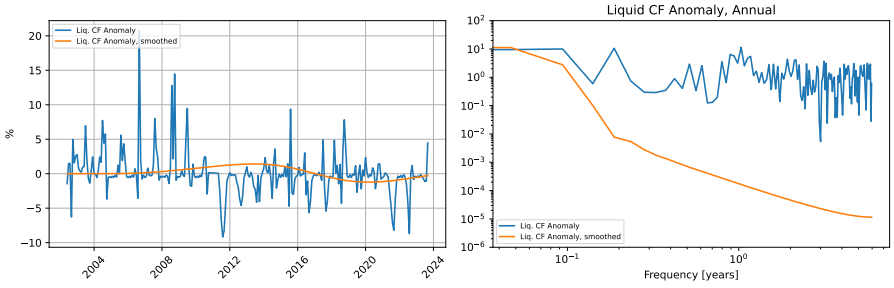

Figure B1. Timeseries of the un-altered and 10 year low-pass smoothed liquid temporal cloud fraction anomaly in panel a), with a power spectra decomposition of these curves in panel b).

of this timeseries found in Fig. B1b. A strong signal is seen with a period of 9 years, which we damp by applying a 10 year low-pass filter to the timeseries, with the resulting timeseries and power spectra overlaid on Fig. B1a and Fig. B1b in orange. A significant amount of high frequency noise in the data is due to the preferential filtering out of winter retrievals required by our quality control limitations, as discussed in Sect. 2. In order to apply our filter, interpolation over gaps in our data are necessary to preserve the temporal frequency of monthly cloud fraction anomalies. A cubic spline interpolation was performed to create Figures B1 and 4, as well as Tab. D1. Other interpolation methods were tested and we found minimal impact on the values of Tab. D1 with no qualitative impact on the conclusions presented in Fig. 4 and Sect. 3.2.

Appendix C: Empirical Cumulative Distribution Function of Liquid Water Path in the MIXCRA dataset

In order to provide a direct comparison between the subset of clouds that we study to all clouds observed over the NSA site, empirical cumulative distribution functions (ECDF) of LWP were generated for the MIXCRA dataset as well as for the LWP as measured by a microwave radiometer (MWR) at the NSA site (Zhang, 2025), which is able to capture a much larger range of LWPs, despite it's much larger uncertainty at low LWP (Turner, 2007). The MWR ECDF is made up of data from January 2012 to August 2023, while the MIXCRA ECDF contains all available data (April 2002 to August 2023). The clouds that we study in this manuscript are of a subset of clouds with a much smaller LWP than the typical cloud observed over the NSA site.

Appendix D: Cloud feedback analysis values and coefficients of determination

The Gregory regression of local surface cloud radiative effect anomalies against global surface temperature anomalies which constitutes the surface cloud feedback (Gregory et al., 2004) produces a slope and a coefficient of determination. The slope of this linear regression is the value of the feedback, determining its magnitude and sign, while the coefficient of determination describes how much of the total variance in local surface cloud radiative effect anomaly can be explained by global surface temperature anomaly. These metrics, associated with our cloud feedback analysis in Fig. 4, are collected in Tab. D1 for all seasons and feedbacks.

https://doi.org/10.5194/egusphere-2025-6553
Preprint. Discussion started: 8 January 2026

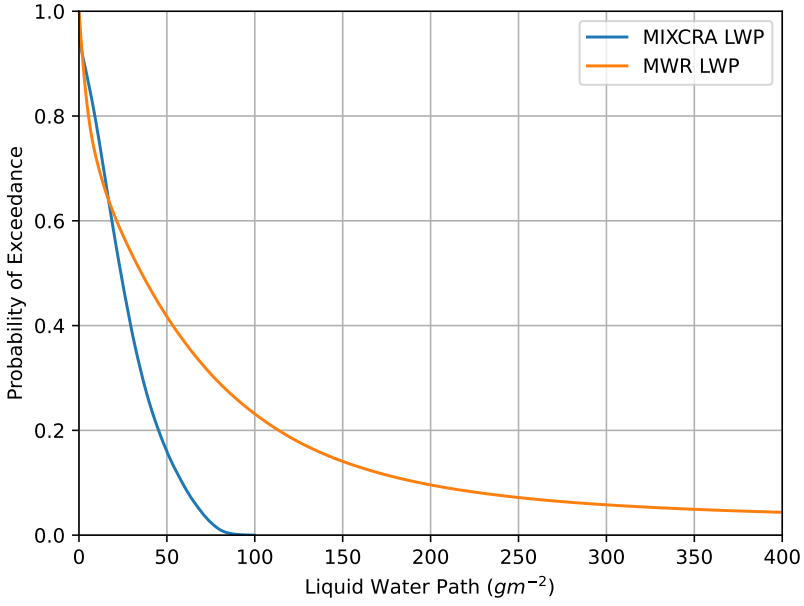

Figure C1. Empirical cumulative distribution functions of liquid water path as retrieved by the MIXCRA algorithm and a collocated microwave radiometer (MWR).

Table D1. Collected values of each individual feedback parameter in Fig. 4, and coefficient of determination as calculated via Gregory regression (Gregory et al., 2004).

	Annual		Winter		Spring		Summer		Autumn	
	Slope	r^2	Slope	r^2	Slope	r^2	Slope	r^2	Slope	r^2
SW Liq.	0.78	0.29	0.02	0.19	0.57	0.31	1.46	0.17	0.54	0.30
LW Liq.	-1.87	0.29	-1.59	0.28	-1.71	0.29	-1.37	0.16	-2.20	0.30
SW Ice	0.07	0.13	0.00	0.30	0.06	0.16	0.10	0.04	0.06	0.15
LW Ice	-0.19	0.13	-0.23	0.29	-0.18	0.15	-0.09	0.03	-0.22	0.14
Net	-1.20	NA	-1.80	NA	-1.26	NA	0.09	NA	-1.82	NA

https://doi.org/10.5194/egusphere-2025-6553
Preprint. Discussion started: 8 January 2026

Author contributions. CC retrieved the dataset of cloud optical depth, performed analyses and aided in their interpretation, and prepared the manuscript. DT provided guidance on the usage and interpretation of the results of the MIXCRA algorithm and wrote passages on the MIXCRA algorithm in Sect. 2. IT conceptualized the project and its methodology, supervised the analysis and writing of the manuscript, and acquired funding for this work. CZ provided the cloud radiative kernel dataset. All authors reviewed the writing of the manuscript.

Competing interests. The authors declare that they have no conflict of interest

Acknowledgements. This work was supported by the U.S. Department of Energy Atmospheric System Research program under award DE-SC0023056. The scientific results and conclusions, as well as any views or opinions expressed herein, are those of the author(s) and do not necessarily reflect those of NOAA or the Department of Commerce.

https://doi.org/10.5194/egusphere-2025-6553
Preprint. Discussion started: 8 January 2026

References

Allan, R. P.: Combining satellite data and models to estimate cloud radiative effect at the surface and in the atmosphere, Meteorological Applications, 18, 324–333, https://doi.org/https://doi.org/10.1002/met.285, 2011.

Anderson, G. P., Clough, S. A., Kneizys, F. X., Chetwynd, J. H., and Shettle, E. P.: AFGL atmospheric constituent profiles (0.120km), 1986.

Bi, H., Wang, Y., Liang, Y., Sun, W., Liang, X., Yu, Q., Zhang, Z., and Xu, X.: Influences of Summertime Arctic Dipole Atmospheric Circulation on Sea Ice Concentration Variations in the Pacific Sector of the Arctic during Different Pacific Decadal Oscillation Phases, Journal of Climate, 34, 3003 – 3019, https://doi.org/10.1175/JCLI-D-19-0843.1, 2021.

Blanchard, Y., Pelon, J., Eloranta, E. W., Moran, K. P., Delanoë, J., and Sèze, G.: A Synergistic Analysis of Cloud Cover and Vertical Distribution from A-Train and Ground-Based Sensors over the High Arctic Station Eureka from 2006 to 2010, Journal of Applied Meteorology and Climatology, 53, https://doi.org/https://doi.org/10.1175/JAMC-D-14-0021.1, 2014.

Blossey, P. N., Bretherton, C. S., Zhang, M., Cheng, A., Endo, S., Heus, T., Liu, Y., Lock, A. P., de Roode, S. R., and Xu, K.-M.: Marine low cloud sensitivity to an idealized climate change: The CGILS LES intercomparison, Journal of Advances in Modeling Earth Systems, 5, 234–258, https://doi.org/https://doi.org/10.1002/jame.20025, 2013.

Bretherton, C. S. and Wyant, M. C.: Moisture Transport, Lower-Tropospheric Stability, and Decoupling of Cloud-Topped Boundary Layers, Journal of the Atmospheric Sciences, 54, 148 – 167, https://doi.org/10.1175/1520-0469(1997)054<0148:MTLTSA>2.0.CO;2, 1997.

Ceppi, P. and Nowack, P.: Observational evidence that cloud feedback amplifies global warming, Proceedings of the National Academy of Sciences, 118, https://doi.org/10.1073/pnas.2026290118, 2021.

Ceppi, P., Brient, F., Zelinka, M. D., and Hartmann, D. L.: Cloud feedback mechanisms and their representation in global climate models, WIREs Climate Change, 8, https://doi.org/https://doi.org/10.1002/wcc.465, 2017.

Chan, M. A. and Comiso, J. C.: Arctic Cloud Characteristics as Derived from MODIS, CALIPSO, and CloudSat, Journal of Climate, 26, 3285 – 3306, https://doi.org/10.1175/JCLI-D-12-00204.1, 2013.

Clough, S., Shephard, M., Mlawer, E., Delamere, J., Iacono, M., Cady-Pereira, K., Boukabara, S., and Brown, P.: Atmospheric radiative transfer modeling: a summary of the AER codes, Journal of Quantitative Spectroscopy and Radiative Transfer, 91, 233–244, https://doi.org/https://doi.org/10.1016/j.jqsrt.2004.05.058, 2005.

Coulbury, C. and Tan, I.: Top of the atmosphere shortwave Arctic cloud feedbacks: A comparison of diagnostic methods, Geophysical Research Letters, 51, https://doi.org/https://doi.org/10.1029/2023GL107780, 2024.

Curry, J. A., Schramm, J. L., Rossow, W. B., and Randall, D.: Overview of Arctic Cloud and Radiation Characteristics, Journal of Climate, 9, 1731 – 1764, https://doi.org/10.1175/1520-0442(1996)009<1731:OOACAR>2.0.CO;2, 1996.

Dai, A., Luo, D., Song, M., and Liu, J.: Arctic amplification is caused by sea-ice loss under increasing CO2, Nature Communications, 10, https://doi.org/https://doi.org/10.1038/s41467-018-07954-9, 2019.

Dee, D. P., Uppala, S. M., Simmons, A. J., Berrisford, P., Poli, P., Kobayashi, S., Andrae, U., Balmaseda, M. A., Balsamo, G., Bauer, P., Bechtold, P., Beljaars, A. C. M., van de Berg, L., Bidlot, J., Bormann, N., Delsol, C., Dragani, R., Fuentes, M., Geer, A. J., Haimberger, L., Healy, S. B., Hersbach, H., Hólm, E. V., Isaksen, L., Kållberg, P., Köhler, M., Matricardi, M., McNally, A. P., Monge-Sanz, B. M., Morcrette, J.-J., Park, B.-K., Peubey, C., de Rosnay, P., Tavolato, C., Thépaut, J.-N., and Vitart, F.: The ERA-Interim reanalysis: configuration and performance of the data assimilation system, Quarterly Journal of the Royal Meteorological Society, 137, 553–597, https://doi.org/https://doi.org/10.1002/qj.828, 2011.

https://doi.org/10.5194/egusphere-2025-6553
Preprint. Discussion started: 8 January 2026

Deslover, D. H., Smith, W. L., Piironen, P. K., and Eloranta, E. W.: A methodology for measuring cirrus cloud visible-to-infrared spectral optical depth ratios, J. Atmos. Oceanic Technol., 16, 251–262, 1999.

Gettelman, A. and Sherwood, S. C.: Processes Responsible for Cloud Feedback, Current Climate Change Reports, 2, https://doi.org/https://doi.org/10.1007/s40641-016-0052-8, 2016.

Global Modeling and Assimilation Office (GMAO): MERRA-2 inst3_3d_aer_nv: 3D, 3-hourly, instantaneous, model-level, assimilation, aerosol mixing ratio V5.12.4, https://doi.org/https://doi.org/10.5067/LTVB4GPCOTK2, 2015.

Gordon, N. D. and Klein, S. A.: Low-cloud optical depth feedback in climate models, Journal of Geophysical Research: Atmospheres, 119, https://doi.org/https://doi.org/10.1002/2013JD021052, 2014.

Gregory, J. M., Ingram, W. J., Palmer, M. A., Jones, G. S., Stott, P. A., Thorpe, R. B., Lowe, J. A., Johns, T. C., and Williams, K. D.: A new method for diagnosing radiative forcing and climate sensitivity, Geophysical Research Letters, 31, https://doi.org/https://doi.org/10.1029/2003GL018747, 2004.

Grenfell, T. C. and Warren, S. G.: Representation of a nonspherical ice particle by a collection of independent spheres for scattering and absorption of radiation, Journal of Geophysical Research: Atmospheres, 104, 31 697–31 709, 1999.

Hahn, L. C., Armour, K. C., Zelinka, M. D., Bitz, C. M., and Donohoe, A.: Contributions to Polar Amplification in CMIP5 and CMIP6, Frontiers in Earth Science, 9, https://doi.org/https://doi.org/10.3389/feart.2021.710036, 2021.

Jenkins, M. and Dai, A.: The Impact of Sea-Ice Loss on Arctic Climate Feedbacks and Their Role for Arctic Amplification, Geophysical Research Letters, 48, https://doi.org/https://doi.org/10.1029/2021GL094599, 2021.

Kanji, Z. A., Ladino, L. A., Wex, H., Boose, Y., Burkert-Kohn, M., Cziczo, D. J., and Krämer, M.: Overview of Ice Nucleating Particles, Meteorological Monographs, 58, 1.1 – 1.33, https://doi.org/10.1175/AMSMONOGRAPHS-D-16-0006.1, 2017.

Klein, S., Hall, A., and Norris, J.: Low-Cloud Feedbacks from Cloud-Controlling Factors: A Review, Surveys in Geophysics, 38, 1307–1329, https://doi.org/https://doi.org/10.1007/s10712-017-9433-3, 2017.

Knuteson, R. O., Revercomb, H. E., Best, F. A., Ciganovich, N. C., Dedecker, R. G., Dirkx, T. P., Ellington, S. C., Feltz, W. F., Garcia, R. K., Howell, H. B., Smith, W. L., Short, J. F., and Tobin, D. C.: Atmospheric Emitted Radiance Interferometer. Part I: Instrument Design, Journal of Atmospheric and Oceanic Technology, 21, 1763 – 1776, https://doi.org/10.1175/JTECH-1662.1, 2004a.

Knuteson, R. O., Revercomb, H. E., Best, F. A., Ciganovich, N. C., Dedecker, R. G., Dirkx, T. P., Ellington, S. C., Feltz, W. F., Garcia, R. K., Howell, H. B., Smith, W. L., Short, J. F., and Tobin, D. C.: Atmospheric Emitted Radiance Interferometer. Part II: Instrument Performance, Journal of Atmospheric and Oceanic Technology, 21, 1777 – 1789, https://doi.org/10.1175/JTECH-1663.1, 2004b.

Korolev, A., McFarquhar, G., Field, P. R., Franklin, C., Lawson, P., Wang, Z., Williams, E., Abel, S. J., Axisa, D., Borrmann, S., Crosier, J., Fugal, J., Krämer, M., Lohmann, U., Schlenczek, O., Schnaiter, M., and Wendisch, M.: Mixed-Phase Clouds: Progress and Challenges, Meteorological Monographs, 58, 5.1 – 5.50, https://doi.org/10.1175/AMSMONOGRAPHS-D-17-0001.1, 2017.

Lawson, R. P., Baker, B. A., Schmitt, C. G., and Jensen, T. L.: An overview of microphysical properties of Arctic clouds observed in May and July 1998 during FIRE ACE, Journal of Geophysical Research: Atmospheres, 106, https://doi.org/https://doi.org/10.1029/2000JD900789, 2001.

Liu, L., Huang, Y., Gyakum, J. R., Turner, D. D., and Gero, P. J.: Trends in Downwelling Longwave Radiance Over the Southern Great Plains, Journal of Geophysical Research: Atmospheres, 127, https://doi.org/https://doi.org/10.1029/2021JD035949, 2022.

Liu, Z., Vaughan, M., Winker, D., Kittaka, C., Getzewich, B., Kuehn, R., Omar, A., Powell, K., Trepte, C., and Hostetler, C.: The CALIPSO Lidar Cloud and Aerosol Discrimination: Version 2 Algorithm and Initial Assessment of Performance, Journal of Atmospheric and Oceanic Technology, 26, https://doi.org/https://doi.org/10.1175/2009JTECHA1229.1, 2009.

https://doi.org/10.5194/egusphere-2025-6553
Preprint. Discussion started: 8 January 2026

Maahn, M., Turner, D. D., Löhnert, U., Posselt, D. J., Ebell, K., Mace, G. G., and Comstock, J. M.: Optimal estimation retrievals and their uncertainties: What every atmospheric scientist should know, Bulletin of the American Meteorological Society, 101, E1512–E1523, 2020.

Mace, G. G., Ackerman, T. P., Minnis, P., and Young, D. F.: Cirrus layer microphysical properties derived from surface-based millimeter radar and infrared interferometer data, J. Geophys. Res., 103, 23–23, 1998.

Manabe, S. and Stouffer, R. J.: Sensitivity of a global climate model to an increase of CO2 concentration in the atmosphere, Journal of Geophysical Research: Oceans, 85, 5529–5554, https://doi.org/https://doi.org/10.1029/JC085iC10p05529, 1980.

McCoy, D. T., Eastman, R., Hartmann, D. L., and Wood, R.: The Change in Low Cloud Cover in a Warmed Climate Inferred from AIRS, MODIS, and ERA-Interim, Journal of Climate, 30, 3609 – 3620, https://doi.org/10.1175/JCLI-D-15-0734.1, 2017.

Mioche, G., Jourdan, O., Delanoë, J., Gourbeyre, C., Febvre, G., Dupuy, R., Monier, M., Szczap, F., Schwarzenboeck, A., and Gayet, J.-F.: Vertical distribution of microphysical properties of Arctic springtime low-level mixed-phase clouds over the Greenland and Norwegian seas, Atmospheric Chemistry and Physics, 17, 12 845–12 869, https://doi.org/10.5194/acp-17-12845-2017, 2017.

Mlawer, E. J., Taubman, S. J., Brown, P. D., Iacono, M. J., and Clough, S. A.: Radiative transfer for inhomogeneous atmospheres: RRTM, a validated correlated-k model for the longwave, Journal of Geophysical Research: Atmospheres, 102, 16 663–16 682, https://doi.org/https://doi.org/10.1029/97JD00237, 1997.

Morrison, H., de Boer, G., Feingold, G., Harrington, J., Shupe, M., and Sulia, K.: Resilience of persistent Arctic mixed-phase clouds, Nature Geoscience, 5, 11–17, https://doi.org/https://doi.org/10.1038/ngeo1332, 2012.

Myers, T., Scott, R., and Zelinka, M.: Observational constraints on low cloud feedback reduce uncertainty of climate sensitivity, Nature Climate CHange, 11, 501–507, https://doi.org/https://doi.org/10.1038/s41558-021-01039-0, 2021.

Naud, C. M., Elsaesser, G. S., and Booth, J. F.: Dominant Cloud Controlling Factors for Low-Level Cloud Fraction: Subtropical Versus Extratropical Oceans, Geophysical Research Letters, 50, https://doi.org/https://doi.org/10.1029/2023GL104496, 2023.

Pithan, F., Medeiros, B., and Mauritsen, T.: Mixed-phase Clouds Cause Climate Model Biases in Arctic Wintertime Temperature Inversions, Climate Dynamics, 43, 289–303, 2014.

Previdi, M., Smith, K. L., and Polvani, L. M.: Arctic amplification of climate change: a review of underlying mechanisms, Environmental Research Letters, 16, https://doi.org/10.1088/1748-9326/ac1c29, 2021.

Qu, X., Hall, A., Klein, S. A., and DeAngelis, A. M.: Positive tropical marine low-cloud cover feedback inferred from cloud-controlling factors, Geophysical Research Letters, 42, 7767–7775, https://doi.org/https://doi.org/10.1002/2015GL065627, 2015.

Rantanen, M., Karpechko, A. Y., Lipponen, A., Nordling, K., Hyvärinen, O., Ruosteenoja, K., Vihma, T., and Laaksonen, A.: The Arctic has warmed nearly four times faster than the globe since 1979, Communications Earth & Environment, 3, https://doi.org/https://doi.org/10.1038/s43247-022-00498-3, 2022.

Rodgers, C. D.: Inverse methods for atmospheric sounding: theory and practice, vol. 2, World scientific, 2000.

Stamnes, K., Tsay, S.-C., Wiscombe, W., and Jayaweera, K.: Numerically stable algorithm for discrete-ordinate-method radiative transfer in multiple scattering and emitting layered media, Applied Optics, 27, 2502–2509, https://doi.org/10.1364/AO.27.002502, 1988.

Stauffer, C. L., Tan, I., and Matrosov, S. Y.: Aerosol and Meteorological Influences on Mixed-Phase Stratiform Clouds at North Slope of Alaska, Geophysical Research Letters, 52, https://doi.org/https://doi.org/10.1029/2025GL114815, 2025.

Stephens, G. L.: Radiation Profiles in Extended Water Clouds. II: Parameterization Schemes, Journal of Atmospheric Sciences, 35, 2123 – 2132, https://doi.org/10.1175/1520-0469(1978)035<2123:RPIEWC>2.0.CO;2, 1978.

Stephens, G. L.: Remote Sensing of the Lower Atmosphere: An Introduction, Oxford University Press, 1994.

https://doi.org/10.5194/egusphere-2025-6553
Preprint. Discussion started: 8 January 2026

Sun, J. and Ariya, P. A.: Atmospheric organic and bio-aerosols as cloud condensation nuclei (CCN): A review, Atmospheric Environment, 40, 795–820, https://doi.org/https://doi.org/10.1016/j.atmosenv.2005.05.052, 2006.

Sun, Z. and Shine, K. P.: Studies of the radiative properties of ice and mixed-phase clouds, Quarterly Journal of the Royal Meteorological Society, 120, 111–137, https://doi.org/https://doi.org/10.1002/qj.49712051508, 1994.

Tan, I., Storelvmo, T., and Choi, Y.-S.: Spaceborne lidar observations of the ice-nucleating potential of dust, polluted dust, and smoke aerosols in mixed-phase clouds, Journal of Geophysical Research: Atmospheres, 119, 6653–6665, https://doi.org/https://doi.org/10.1002/2013JD021333, 2014.

Tan, I., Storelvmo, T., and Zelinka, M. D.: Observational constraints on mixed-phase clouds imply higher climate sensitivity, Science, 352, 224–227, 2016.

Tan, I., Oreopoulos, L., and Cho, N.: The Role of Thermodynamic Phase Shifts in Cloud Optical Depth Variations With Temperature, Geophysical Research Letters, 46, https://doi.org/https://doi.org/10.1029/2018GL081590, 2019.

Tan, I., Barahona, D., and Coopman, Q.: Potential Link Between Ice Nucleation and Climate Model Spread in Arctic Amplification, Geophysical Research Letters, 49, https://doi.org/https://doi.org/10.1029/2021GL097373, 2022.

Tan, I., Zelinka, M. D., Coopman, Q., Kahn, B. H., Oreopoulos, L., Tselioudis, G., McCoy, D. T., and Li, N.: Contributions From Cloud Morphological Changes to the Interannual Shortwave Cloud Feedback Based on MODIS and ISCCP Satellite Observations, Journal of Geophysical Research: Atmospheres, 129, https://doi.org/https://doi.org/10.1029/2023JD040540, 2024a.

Tan, I., Zelinka, M. D., Coopman, Q., Kahn, B. H., Oreopoulos, L., Tselioudis, G., McCoy, D. T., and Li, N.: Contributions From Cloud Morphological Changes to the Interannual Shortwave Cloud Feedback Based on MODIS and ISCCP Satellite Observations, Journal of Geophysical Research: Atmospheres, 129, https://doi.org/https://doi.org/10.1029/2023JD040540, 2024b.

Taylor, P. C., Boeke, R. C., Boisvert, L. N., Feldl, N., Henry, M., Huang, Y., Langen, P. L., Liu, W., Pithan, F., Seias, S. A., and Tan, I.: Process Drivers, Inter-Model Spread, and the Path Forward: A Review of Amplified Arctic Warming, Frontiers in Earth Science, 9, https://doi.org/https://doi.org/10.3389/feart.2021.758361, 2022.

Terai, C. R., Zhang, Y., Klein, S. A., Zelinka, M. D., Chiu, J. C., and Min, Q.: Mechanisms Behind the Extratropical Stratiform Low-Cloud Optical Depth Response to Temperature in ARM Site Observations, Journal of Geophysical Research: Atmospheres, 124, 2127–2147, https://doi.org/https://doi.org/10.1029/2018JD029359, 2019.

Tiao, G. C., Reinsel, G. C., Xu, D., Pedrick, J. H., Zhu, X., Miller, A. J., DeLuisi, J. J., Mateer, C. L., and Wuebbles, D. J.: Effects of autocorrelation and temporal sampling schemes on estimates of trend and spatial correlation, Journal of Geophysical Research: Atmospheres, 95, 20 507–20 517, https://doi.org/https://doi.org/10.1029/JD095iD12p20507, 1990.

Tseloudis, G., Rossow, W. B., and Rind, D.: Global Patterns of Cloud Optical Thickness Variation with Temperature, Journal of Climate, 5, 1992.

Turner, D. D.: Microphysical properties of single and mixed-phase Arctic clouds derived from ground-based AERI observations, The University of Wisconsin-Madison, 2003.

Turner, D. D.: Arctic Mixed-Phase Cloud Properties from AERI Lidar Observations: Algorithm and Results from SHEBA, Journal of Applied Meteorology, 44(4):427-444, 44, https://doi.org/10.1175/JAM2208.1, 2005.

Turner, D. D.: Improved ground-based liquid water path retrievals using a combined infrared and microwave approach, Journal of Geophysical Research: Atmospheres, 112, https://doi.org/https://doi.org/10.1029/2007JD008530, 2007.

Turner, D. D. and Eloranta, E. W.: Validating Mixed-Phase Cloud Optical Depth Retrieved From Infrared Observations With High Spectral Resolution Lidar, IEEE Geoscience and Remote Sensing Letters, 5, 285–288, https://doi.org/10.1109/LGRS.2008.915940, 2008.

https://doi.org/10.5194/egusphere-2025-6553
Preprint. Discussion started: 8 January 2026

Turner, D. D., Knuteson, R. O., Revercomb, H. E., Lo, C., and Dedecker, R. G.: Noise Reduction of Atmospheric Emitted Radiance Interferometer (AERI) Observations Using Principal Component Analysis, Journal of Atmospheric and Oceanic Technology, 23, 1223 – 1238, https://doi.org/10.1175/JTECH1906.1, 2006.

Turner, D. D., Vogelmann, A. M., Austin, R. T., Barnard, J. C., Cady-Pereira, K., Chiu, J. C., Clough, S. A., Flynn, C., Khaiyer, M. M., Liljegren, J., Johnson, K., Lin, B., Long, C., Marshak, A., Matrosov, S. Y., McFarlane, S. A., Miller, M., Min, Q., Minimis, P., O'Hirok, W., Wang, Z., and Wiscombe, W.: Thin Liquid Water Clouds: Their Importance and Our Challenge, Bulletin of the American Meteorological Society, 88, 177 – 190, https://doi.org/10.1175/BAMS-88-2-177, 2007.

Turner, D. D., Mlawer, E. J., and Revercomb, H. E.: Water Vapor Observations in the ARM Program, Meteorological Monographs, 57, 13.1 – 13.18, https://doi.org/10.1175/AMSMONOGRAPHS-D-15-0025.1, 2016.

Verlinde, J., Zak, B. D., Shupe, M. D., Ivey, M. D., and Stamnes, K.: The ARM North Slope of Alaska (NSA) Sites, Meteorological Monographs, 57, 8.1 – 8.13, https://doi.org/10.1175/AMSMONOGRAPHS-D-15-0023.1, 2016.

Weatherhead, E. C., Reinsel, G. C., Tiao, G. C., Meng, X.-L., Choi, D., Cheang, W.-K., Keller, T., DeLuisi, J., Wuebbles, D. J., Kerr, J. B., Miller, A. J., Oltmans, S. J., and Frederick, J. E.: Factors affecting the detection of trends: Statistical considerations and applications to environmental data, Journal of Geophysical Research: Atmospheres, 103, 17 149–17 161, https://doi.org/https://doi.org/10.1029/98JD00995, 1998.

Winker, D. M., Vaughan, M. A., Omar, A., Hu, Y., Powell, K. A., Liu, Z., Hunt, W. H., and Young, S. A.: Overview of the CALIPSO Mission and CALIOP Data Processing Algorithms, Journal of Atmospheric and Oceanic Technology, 26, https://doi.org/https://doi.org/10.1175/2009JTECHA1281.1, 2009.

Wolf, V., Kuhn, T., Milz, M., Voelger, P., Krämer, M., and Rolf, C.: Arctic ice clouds over northern Sweden: microphysical properties studied with the Balloon-borne Ice Cloud particle Imager B-ICI, Atmospheric Chemistry and Physics, 18, 17 371–17 386, https://doi.org/10.5194/acp-18-17371-2018, 2018.

Yang, P., Wei, H., Huang, H.-L., Baum, B. A., Hu, Y. X., Kattawar, G. W., Mishchenko, M. I., and Fu, Q.: Scattering and absorption property database for nonspherical ice particles in the near- through far-infrared spectral region, Applied Optics, 44, 5512–5523, https://doi.org/10.1364/AO.44.005512, 2005.

Zelinka, M., Klein, S., and Hartmann, D.: Computing and Partitioning Cloud Feedbacks Using Cloud Property Histograms. Part I: Cloud Radiative Kernels, Journal of Climate, 25, https://doi.org/doi:10.1175/JCLI-D-11-00248.1, 2012.

Zhang, D.: MWR Retrievals (MWRRET1LILJCLOU), 2011-01-01 to 2025-06-26, North Slope Alaska (NSA), Central Facility, Barrow AK (C1), 2025.

Zhang, D., Vogelmann, A., Kollias, P., Luke, E., Yang, F., Lubin, D., and Wang, Z.: Comparison of Antarctic and Arctic Single-Layer Stratiform Mixed-Phase Cloud Properties Using Ground-Based Remote Sensing Measurements, Journal of Geophysical Research: Atmospheres, 124, 10 186–10 204, https://doi.org/https://doi.org/10.1029/2019JD030673, 2019.

Zhou, C., Liu, Y., and Wang, Q.: Calculating the Climatology and Anomalies of Surface Cloud Radiative Effect Using Cloud Property Histograms and Cloud Radiative Kernels, Advances in Atmopsheric Sciences, 39, https://doi.org/https://doi.org/10.1007/s00376-021-1166-z., 2022.

Zwink, A. B. and Turner, D. D.: Using a Neural Network to Determine the Hatch Status of the AERI at the ARM North Slope of Alaska Site, ARM User Facility, https://doi.org/DOE/SC-ARM-TR-107, 2012.